analytical chemistry

pubs.acs.org/ac Review

Laser-Induced Breakdown Spectroscopy Imaging for Material and Biomedical Applications: Recent Advances and Future Perspectives

Vincent Gardette, Vincent Motto-Ros, César Alvarez-Llamas, Lucie Sancey, Ludovic Duponchel, and Benoit Busser*

Cite This: *Anal. Chem.* 2023, 95, 49–69 Read Online

CONTENTS

Laser-induced breakdown spectroscopy (LIBS) is a versatile analytical tool for studying the elemental composition of any kind of sample, such as solids, liquids, or gases. One of the latest developments in this technique is the ability to use it for elemental imaging, that is to say spatially resolved surface analysis. LIBS imaging is becoming a very attractive and popular technique for the qualitative and/or quantitative spectrochemical characterization of specimens for a wide range of applications. Because of its unique set of intrinsic advantages, LIBS imaging is frequently preferred over competitive and complementary techniques for elemental imaging. This review recapitulates the technical fundamentals of LIBS imaging and focuses on significant applications that have received the most promising attention and have undergone major advances during the last three years in the industrial, geological, and biomedical fields. We also discuss the current limitations that hinder the further development of LIBS imaging, as well as perspectives on the use of LIBS as a part of multimodal imaging strategies, the contribution of chemometrics, and ideas for improving the limits of detection and quantification aspects.

In the past few years, the application of laser-induced breakdown spectroscopy in microscopic elemental imaging has been steadily increasing. The recent improvement in its performance makes this technology more and more attractive for many application fields, including biomedical, geological material analysis, and industry.[1−5] In LIBS-based imaging, a laser-induced plasma is generated at different locations of a sample with a pattern covering the region of interest. Such a plasma source allows specific optical responses resulting from the relaxation of atoms and ions excited by the high plasma temperature to be elicited.[6,7] The major advantage of this approach is that it is possible to perform an elemental measurement from a single laser pulse, which simultaneously samples the material (by laser ablation) atomizes and then excites the ablated vapor by heating the plasma. This facilitates unique features of LIBS-based imaging with a series of advantages, including simple instrumentation, operation at ambient pressure and temperature, a fast operating speed (up to kHz), and an all-optical design, fully compatible with conventional optical microscopy. Such compatibility plays a facilitating role in coupling LIBS imaging with other techniques, such as Raman spectroscopy and/or luminescence. In addition to having a table-top instrumentation, LIBS

Special Issue: Fundamental and Applied Reviews in Analytical Chemistry 2023

Published: January 10, 2023

https://doi.org/10.1021/acs.analchem.2c04910
Anal. Chem. 2023, 95, 49−69

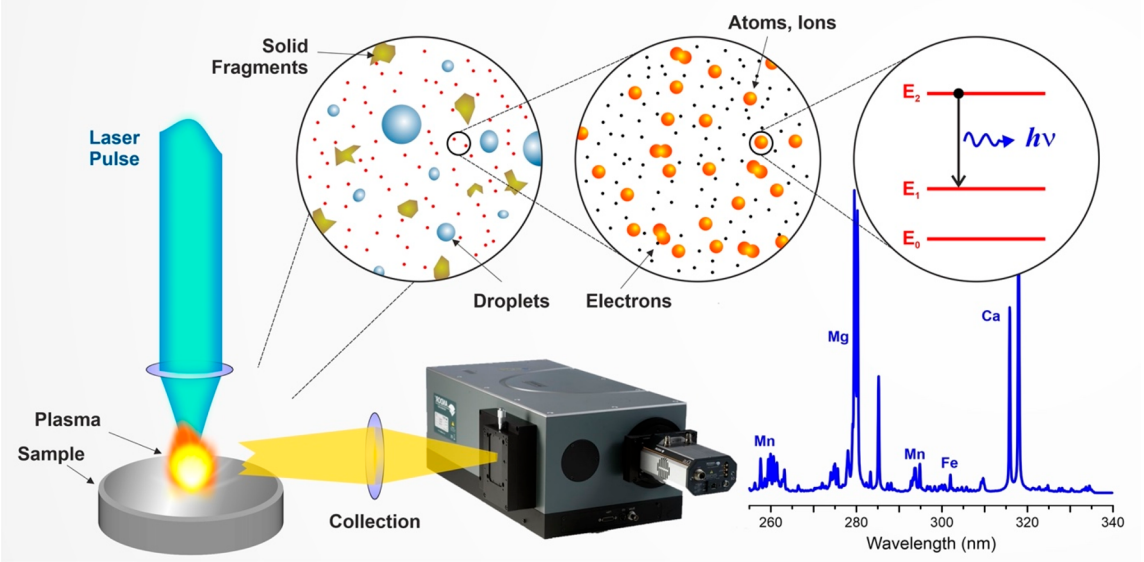

Figure 1. Physical principle of the LIBS technique. Adapted with permission from *Spectrochimica Acta Part B: Atomic Spectroscopy* vol 166, Fabre, C. Advances in Laser-Induced Breakdown Spectroscopy Analysis for Geology: A Critical Review. 105799 (ref 24). Copyright 2020, with permission from Elsevier.

imaging also has valuable analytical figures of merit, such as no restrictions in the detection of light elements, multielemental capabilities, limit of detection (LoD) in the range of ppm for most of the elements, and microscopic-scale resolution.[2] All these advantages make LIBS imaging very promising, with the potential to become a reference technique for highly sensitive and spatially resolved elemental approaches, with good complementarities with gold standard methods, such as LA-ICP−MS, synchrotron radiation microanalysis (μXRF), or electron probe microanalysis (EPMA).[8−11]

The possibility of performing spatially rapid microanalytical measurements by LIBS is not new. In fact, this concept was even at the origin of the first developments related to this technique in the early 1960s.[12] At that time, LIBS instrumental developments were focused on microanalysis, and several companies, such as Zeiss, developed commercial instruments fairly quickly.[13] However, with the arrival of more robust lasers and the first matrix detectors on the market, the method underwent more significant development. In the late 1990s and early 2000s, a significant number of articles were published demonstrating all the potential of this technique and paving the way for the development of various applications. For example, this technique was applied to quantify cerium in ceramics at the micrometer scale,[14] to perform multielemental LIBS imaging at the kHz operating rate to characterize inclusions in steel,[15] to analyze large sample surfaces,[16,17] and to perform three-dimensional analysis.[18] In the early 2010s, the arrival to the market of new intensified charge coupled device (ICCD) detectors, both faster and more sensitive, truly boosted the development of LIBS-based imaging. This period resulted in several important contributions. First, biological tissue imaging was perceived by the LIBS community as a small revolution, as it opened new avenues in the highly coveted biomedical application field.[19−21] Second, the possibility of obtaining megapixel images was also considered a technological breakthrough, allowing LIBS imaging to become one of the most fashionable hyperspectral methods.[7,22,23] Finally, what is probably the most important contribution is the amount of work employed to make LIBS imaging technology simple, reliable, and fast to use. This last contribution was made possible by a number of companies worldwide, which have focused on developing integrated, reliable, and robust instruments, allowing the technique to reach a previously unattainable level of maturity. These developments are of great benefit to the scientific community, which has access to increasingly powerful instruments offering the opportunity to open up an ever-wider field of applications. However, managing a constantly increasing quantity of data is becoming increasingly difficult. The processing of a large quantity of data is a current obstacle to the development of this technique and its application outside of the laboratory. For this reason, we have chosen to focus this review both on the description of the application fields that seem to have the most potential and on data processing, especially the use of chemometrics methods, which undoubtedly represent a main research challenge for the coming years. However, as a prelude, the following section describes the key instrumental aspects for the implementation of LIBS imaging experiments.

INSIGHTS INTO LIBS IMAGING

Instrumental Basics. LIBS requires a laser pulse to be focused on the sample of interest to ablate a small amount of material (usually a fraction of a microgram or less) and to create a plasma from the vaporized mass. This laser-induced plasma has a typical lifetime of a few microseconds and a temperature in the range of 10 000 K, allowing the excitation of the vast majority of elements, as well as some radicals formed by recombination during the plasma cooling. As shown in Figure 1, the light emitted by the plasma (containing the elemental signature of the sample) is collected by different optical elements (i.e., lenses, mirrors, and optical fibers) and then analyzed using an optical spectrometer. The intensity of the lines (atomic, ionic, and molecular) observed on the emission spectra is directly related to the elemental composition of the sample.

The principle of LIBS imaging lies in the generation of a series of plasmas at different positions of the sample of interest (Figure 2a).[25] Each spectrum is then processed to identify the

https://doi.org/10.1021/acs.analchem.2c04910
Anal. Chem. 2023, 95, 49−69

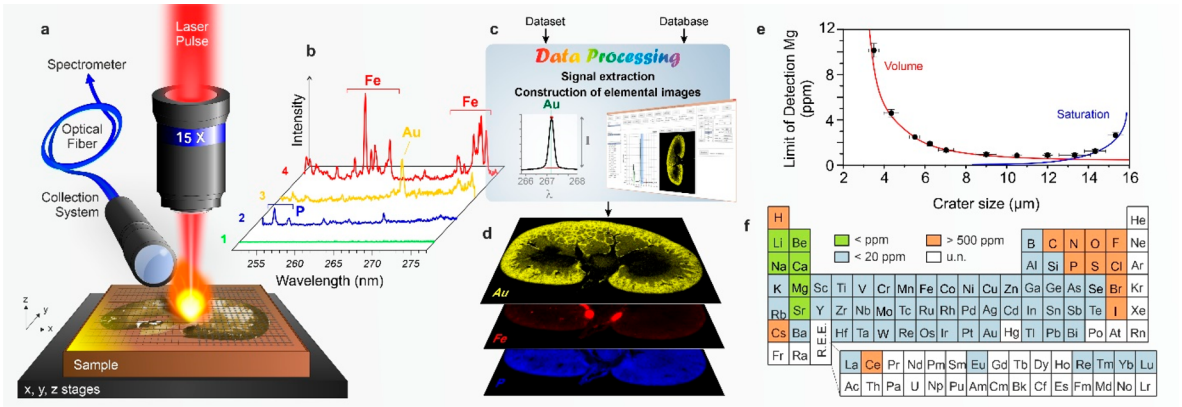

Figure 2. General protocol for LIBS imaging. (a) Schematic view of a micro-LIBS setup showing the major components: the microscope objective used to focus the laser pulse, the motorized platform supporting the sample, and the optical detection system connected to the spectrometer via an optical fiber. (b) Example of single-shot emission spectra covering the 250−280 nm spectral range recorded in different regions of a sample (here, a mouse kidney) with the characteristic emission lines of iron (Fe), phosphorus (P), and gold (Au). (c) Data-processing step, extraction of the relevant signal, and reconstruction of the corresponding elemental images. (d) Example of the relative abundance images of Au (yellow), Fe (red), and P (blue) represented in a false color scale. (e) Evolution of the Mg LoD when reducing the crater size in a configuration using a ×15 magnification lens. (f) Estimated values of the relative detection limits obtained in a single-pulse configuration (u.n.: unknown). Adapted with permission of MJH Life Sciences, from (ref 34).

detected emission lines from the elements of interest and build the corresponding elemental images (Figure 2b−d). For this purpose, the sample is typically positioned on motorized XY stages allowing automated sequences. The lateral resolution or step size (i.e., the distance between consecutive laser shots) then defines the resolution of the final image. In general, the minimal accessible resolution is defined by the crater size. Although it is possible, it is indeed inadvisible to obtain overlaps between consecutive laser shots, since the repeatability of the measurement may be strongly degraded.[26−28] In addition, it seems worth mentioning that in the vast majority of cases, LIBS imaging instruments rely on the movement of the sample instead of scanning it with a mobile laser beam. It is indeed easier to collect the light emitted from a fixed plasma plume position. However, for specific applications requiring the high-frequency-rate scanning of large-sized sample surfaces (such as online control), moving the laser beam continuously along with the collection system appears to be a valuable strategy.[29−33]

Instrumental Configurations. A very large number of possible instrumental configurations is described in the literature. These have recently been reviewed in several review papers,[2,5] and only the more important aspects will be discussed in the following. Briefly, LIBS imaging configurations differ by the choice of (i) the laser focusing parameters; (ii) the laser source and its parameters (wavelength, pulse duration, energy, and pulse frequency or repetition rate); and (iii) the detection system, composed of spectrometers (monochromator, polychromator, compact, echelle, Pashen Runge) and the detectors (ICCD, linear or matrix CCD/CMOS, photomultiplier, etc.)

Laser Focusing. The choice of the focusing system is undoubtedly the most critical one since it will primarily determine the ultimate accessible resolution. Obviously, the shorter the focal length is, the smaller the working distance (WD) and the smaller the crater size. For example, crater diameters smaller than 10 μm may be obtained with a focal length of approximately 15 mm,[6,14] while obtaining crater diameters of approximately 50 μm is relatively easy with a focal length in the range of 100 mm.[29,35,36] In a strong focusing configuration (magnification lens higher than ×10, WD lower than 15 mm), it may become difficult to couple the plasma light efficiently to the spectrometer due to mechanical constraints.[2] The optics (focusing, collection, etc.) also need to be protected from the ejection of dust and/or particles originating from the ablation process.

Moreover, it is easy to appreciate that a smaller crater implies a lower ablated mass, a smaller number of emitters (excited atoms/ions or molecules) in the plasma, and thus a lower measured signal. In such cases, argon gas can be used to flow the plasma region to obtain higher emission properties as the plasma is thermally insulated and better confined compared to that during ablation in air.[37−39] However, there is always a trade-off between resolution and sensitivity (i.e., the LoD). As an example, the evolution of the magnesium (Mg) LoD as a function of the crater diameter is shown in Figure 2e. This result was obtained using a ×15 magnification focusing lens (f = 13.3 mm) in an argon environment on a reference glass by adjusting the laser pulse energy.[34] The LoD strongly deteriorates when reducing the crater size and the corresponding ablated volume. Considering the equivalent plasma generation and excitation capabilities of the laser pulse, a change from 10 to 1 μm in the crater diameter (as well as the depth) may degrade the LoD by approximately 3 orders of magnitude. This suggests how to obtain a LoD within a few percent of that obtained in the work of Wang et al., contrasting with the impressive lateral resolution of less than one micrometer.[40] In this experiment, the laser fluence was maintained under the breakdown threshold, and a silver tip was used to locally increase the laser electromagnetic field via localized surface plasmon resonance (LSPR), leading to very localized ablation. Other studies have proposed offsetting such losses with an external addition to the experimental setup.[2,5] These approaches work, but at the cost of adding experimental constraints. For example, Ahamer et al. used a femtosecond laser for LIBS imaging, resulting in a high spatial resolution of approximately 6 μm.[39] To compensate for the sensitivity loss, a strategy with a second pulse for the reheating and excitation of the plume was used by the same laboratory.[41]

https://doi.org/10.1021/acs.analchem.2c04910
Anal. Chem. 2023, 95, 49−69

Although the LIBS technique generally requires very little sample preparation, this step is nonetheless crucial.[42] It is indeed necessary for the sample to be perfectly flat and clean, which is generally achievable through a polishing step. A constraint related to the technique is to guarantee the positioning of the surface plane with respect to the focal plane of the optical system throughout the imaging experiment. This aspect is of utmost importance, especially when the laser focusing is strong, since the positioning of the sample surface should be controlled at the scale of the Rayleigh length of the beam ($z_R \approx 20$ μm for a spot diameter of 10 μm).[7] Finally, it is important to emphasize that laser ablation is a powerful process. It is indeed accompanied by thermal diffusion through the sample as well as the generation of a shock wave. Both of these effects might cause much more sample deterioration than ablation itself. This is the case for fragile materials in particular, such as thin biological tissue slices. Consequently, to ensure measurement repeatability, the step size (lateral resolution) may be adapted with regard to the sample-induced damage.

Laser Source. Regarding the choice of laser, the critical factor for obtaining optimal LIBS imaging results is, above all, the laser shot-to-shot stability (in terms of not only energy but also pulse duration and pointing), considering that any source instability leads to fluctuations in plasma generation and thus also in the collected signal. A laser source with significant shot-to-shot variations degrades the measurement repeatability and thus also the quality of the obtained elemental images. In the case of LIBS imaging, the laser shot-to-shot stability is more critical than in the case of LIBS for bulk or homogeneous sample microanalysis, since in the latter case, it is possible to accumulate a burst of LIBS measurements, which may compensate for some of the laser variability.

The laser wavelength also influences the LIBS signals, as, in some cases, it is difficult to induce the breakdown of the analyzed materials under certain experimental conditions of laser fluence with a specific laser wavelength. Indeed, many materials are transparent in the visible and near-infrared ranges (with low absorption coefficients at these wavelengths), while very few materials do not absorb in the UV range.[43,44] In addition, the ablation and plasma dynamics may be drastically different according to the laser wavelength, since plasma plume−laser interaction processes are strongly dependent on the wavelength of the plume, and the plume's predominant physical ionization processes (inverse Bremsstrahlung or photoionization) may vary. For example, plasma has a higher absorptivity in infrared; however, the sample ablation efficiency is higher when using UV lasers. It is initially obvious that the use of UV wavelengths appears more relevant. Unfortunately, this wavelength range is generally accessible only by tripling or quadrupling a Nd:YAG pulse at 1064 nm, resulting in poorer laser emission stability compared with the use of the fundamental wavelength.

In addition, to obtain the best focusing capabilities possible, as close as possible to the diffraction limit, the laser beam quality is important (usually measured as M^2), as well as the diameter of the laser beam before it is focused. The latter can be increased by means of optical elements and/or beam expanders.

Detection System. The choice of detection system (spectrometer and detector) is also a question of compromise. In this case, several parameters, including the spectral resolution, spectral measuring range (multielemental capability), spectrometer brightness (measurement sensitivity), operating speed, and cost,[2] must be taken into account to select the appropriate system for a specific application. Unfortunately, a detection system that is able to optimize all these different aspects does not yet exist. For instance, echelle spectrometers have the great advantage of covering a broad spectral range (in general from UV to near-infrared), providing full capabilities in terms of multielemental detection.[45−48] However, the detection sensitivity (brightness) is rather poor due to the small entrance aperture, typically ϕ 50 μm. In addition, the echelle dispersion may involve the loss of spectral zones located between the diffraction orders. The CCD sensor saturation of one or more emission lines could induce the appearance of "ghost lines" due to CCD blooming. Finally, the acquisition rate is also limited to approximately 1−5 Hz since the detector has to read out the full sensor frame. To combine a high detection sensitivity, high acquisition rate, and broad spectral range, one could use a Paschen−Runge spectrometer. Such spectrometers are suitable for simultaneous multielemental detection with the use of photomultiplier tubes at slits and/or a combination of linear CCD detectors.[49] With such a configuration, these spectrometers can operate with acquisition speeds up to the kHz range.[15,50,51] Due to their robustness, Paschen−Runge spectrometers may constitute a relevant choice for industrial applications. However, they are generally costly and bulky apparatuses and should also be ultimately configured once. Czerny−Turner (CT) spectrometers coupled to matrix detectors (CCD, ICCD, EMCCD, etc.) are undoubtedly the most widespread detection systems used for LIBS mapping experiments.[22,23,28,52] The brightness of such spectrometers is high due to a large entrance slit, and they are generally equipped with 3 to 4 different selectable gratings, ensuring the versatility required for laboratory experiments. In addition, the use of ICCDs as detectors facilitates fast synchronization capabilities, allowing well-resolved temporal measurements to be performed and an acquisition rate of up to 100 Hz.[7] However, the main drawback of CT spectrometers is undeniably their limited spectral detection range, typically with spectral windows from ∼20 nm to ∼80 nm depending on the required resolution. Several groups have proposed associating several CT spectrometers in the same LIBS experiment;[7,53,54] however, this results in greater instrumental complexity and associated costs. The use of compact CT spectrometers (Ocean optics, Avantes, etc.) may also be a good approach. Indeed, they have great advantages of affordability and reduced size, which makes their use possible in a multichannel configuration;[29,30,55−57] however, for certain configurations, the exposition time is not adjustable, which may lead to a higher spectral complexity (all the emission generated during the plasma lifetime is recorded), possibly causing spectral interferences for some emission lines.

Finally, it is important to discuss the operating speed of the detection system (i.e., the number of spectra recorded per second). This is obviously primarily dependent on the laser frequency rate. Currently, we have no difficulty finding lasers on the market between 10 Hz and 1 kHz with enough energy to easily produce laser-induced plasma (>mJ) on almost all types of materials. However, above a certain frequency (typically >200 Hz), traditional ICCD detectors as well as certain types of CCD sensors can no longer keep up. It is thus necessary to work with faster sensors (including faster phosphors depending on the technology) with smaller

https://doi.org/10.1021/acs.analchem.2c04910
Anal. Chem. 2023, 95, 49−69

sensitive areas and/or quantum efficiency. In such cases, less light is collected, which leads to a noticeable loss of sensitivity.

Data Processing. One of the challenging tasks in LIBS imaging is undoubtably data processing. This step basically consists of extracting the relevant information contained in the spectral data set and representing it in the form of image(s) with spatial distribution for the elements of interest. A detailed section dedicated exclusively to this aspect is proposed below (please refer to Processing and Chemometrics in LIBS Imaging). The idea here is to only outline the main difficulties encountered during this phase of data treatment. First, the sample itself may be very complex in terms of composition (with potentially different matrices, as for most geological samples), which leads to different matrix effects that must be taken into account during data processing. Second, it is important to keep in mind that LIBS imaging is based on atomic emission spectroscopy, which may result in a highly complex spectral signal in certain cases. Some elements, such as transition metals (i.e., Fe, Ti, Mo, Ni, etc.) indeed have a large number of emission lines in all wavelength domains (from the UV to NIR range). If one or more of these elements are a constituent of a sample, the corresponding spectra will be very dense from a spectral point of view. Consequently, important spectral interferences may occur and affect the signal extraction of other elemental lines, sometimes the most interesting and valuable ones. In addition, in some cases, due to such interference effects, the sensitivity performance may deteriorate significantly, as the number of available lines of the elements of interest is reduced due to interference, which means that the most sensitive line is not always available. In addition, some emission lines present in the spectra may be affected by a self-absorption phenomenon (i.e., emitted photons are reabsorbed before they can escape from the plasma), resulting in a reduction in the measured intensity.[58,59] This effect can be significant if (i) there are elements present in high concentrations in the plasma (typically > wt %) and (ii) the fundamental level is involved in the line transition. This effect could be advantageous in the case of LIBS imaging because it allows the stretching of the detector dynamic range in terms of detectable concentration (typically 5−6 orders of magnitude, from ppm to tens of percent). Saturation due to self-absorption, involving mainly intense transitions, indeed allows the detection of high concentrations without necessarily saturating the detector. The disadvantage is that the response curve between elemental concentration and line intensity is not linear, at least for high concentrations. These different phenomena increase the data set complexity, in terms of both wavelength and intensity. Such complexity depends on the elements present in the sample and their amounts, which have to be addressed on a case-by-case basis.

Finally, to top it all, the large number of spectra recorded to generate more than one million pixel images[7] results in additional difficulties for handling such large data sets. This quantity of data implies the use of little supervised and fast methods for intensity extraction. It seems obviously unthinkable to manually process a million spectra. Today, there are many different processing methodologies that may or may not include an image-processing phase. They can be broadly classified into two categories of methods: univariate and multivariate. Specifically, for example, a univariate method potentially uses a single given wavelength to generate an image. On the other hand, a multivariate chemometrics method exploits all wavelengths of the spectral domain to generate images. Such methodologies have undergone significant developments in recent years and will be detailed in Processing and Chemometrics in LIBS Imaging.

Quantification. In LIBS-based imaging analysis, the term "quantification" is not truly appropriate, since the measurement is performed in a single-shot configuration, and there are, therefore, no statistics related to the intensity associated with a single pixel of an image. However, several works have reported "semiquantitative" imaging using various types of matrices. The most common calibration method uses reference materials with known concentrations and compositions similar to those of the sample of interest to be analyzed under similar conditions to build calibration models. For example, the quantitative imaging of steel,[60] boron-doped crystalline silicon,[61] glass,[52,53] and biological and other materials[62−64] has already been reported. When reference materials are unavailable, one possibility is to regard the imaging data set as representative of the entire sample volume. The global elemental composition is then retrieved afterward using complementary analytical approaches, such as XRF or ICP-based analysis, and then used to calibrate the imaging experiments in a semiquantitative approach. Several examples of using this strategy, such as those involving Ti-doped sapphire,[65] lithium ore,[29] copper−nickel ore,[31] murine kidney,[66] or heterogeneous catalysts,[67] have been reported. In other cases, additional imaging techniques may be applied to calibrate the LIBS measurements. Trichard et al. used a profile measurement performed with an electron microprobe (EPMA) of palladium (Pd) on a catalyst section.[67] In this work, several lines of Pd with various intensities were exploited to cover the entire concentration range without being affected by self-absorption. An equivalent methodology was used for the characterization of piezoelectric crystals.[68] More recently, the use of EPMA to calibrate both μLIBS and μXRF images was proposed by Fabre et al. to obtain mineralogical maps of the studied geological samples. In addition, Cugerone et al. used LA-ICP−MS analysis to study different positions of samples to calibrate LIBS measurements and quantify the germanium (Ge) in Pb−Zn ore deposits.[69,70]

PROMISING APPLICATIONS

LIBS, in general, has almost limitless applications, but in some cases, qualitative and/or quantitative measurement is not enough, and spatial information is needed. In this section, we highlight a limited number of recent and high-quality research studies that align with the most promising application fields, keeping in mind that the selected articles demonstrate the interest and added value of using LIBS imaging compared to more conventional LIBS bulk analysis.

Industry. The capabilities of LIBS make it uniquely advantageous for industrial applications. The implementation of LIBS in industry started several decades ago and was facilitated by a few researchers. Among them, Reinhard Noll initiated the development of LIBS applications for steel analysis in 1995.[71] He recently reported the use of a full-imaging LIBS system for end-of-life industrial products.[72] The system offers 2D and 3D imaging (from both camera and LIBS) and can localize elements of interest (such as Ta and Cu) within industrial products for their recycling. In addition to this example, we will present some industrial fields in which LIBS imaging has been applied.

Material Analysis for Manufacturing Applications. This section presents several applications related to material

https://doi.org/10.1021/acs.analchem.2c04910
Anal. Chem. 2023, 95, 49−69

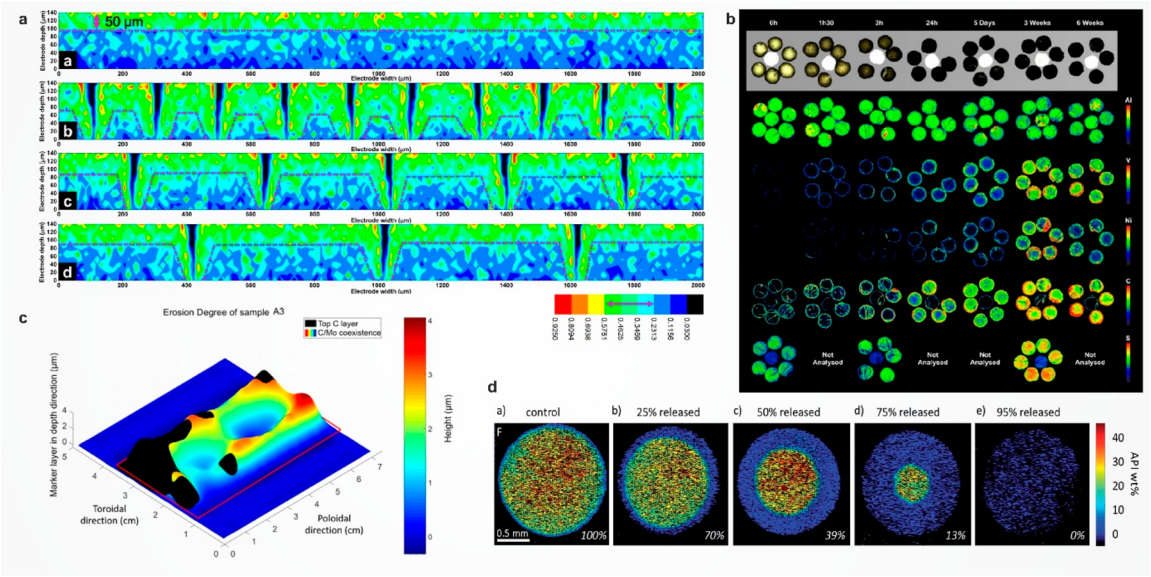

Figure 3. Industrial applications of LIBS imaging. (a) Elemental map of Li from LIBs after different laser patterning. Reprinted from *Journal of Energy Chemistry*, Vol 64, J. Park, H. Song, I. Jang, J. Lee, J. Um, S. Bae, J. Kim, S. Jeong, H-J. Kim. Three-dimensionalization via control of laser-structuring parameters for high energy and high power lithium-ion battery under various operating conditions, 93−102. Copyright 2022, with permission from Elsevier (ref 78). (b) Al, V, Ni, C, and S maps from catalysts. Reprinted from *Applied Surface Science*, Vol 532, R. Yi, D. Zhao, J. Oelmann, S. Brezinsek, M. Rasinski, M. Mayer, C. Prakash Dhard, D. Naujoks, L. Liu, J. Qu. 3-Dimensional analysis of layer structured samples with high depth resolution using picosecond laser-induced breakdown spectroscopy, 147185. Copyright 2020, with permission from Elsevier (ref 81). (c) Quantitative 3D erosion map from graphite tiles after exposure to He/H plasma. Reprinted from *Journal of Catalysis*, Vol 363, F. Trichard, F. Gaulier, J. Barbier, D. Espinat, B. Guichard, C−P. Lienemann, L. Sorbier, P. Levitz, V. Motto-Ros. Imaging of alumina supports by laser-induced breakdown spectroscopy: A new tool to understand the diffusion of trace metal impurities, 183−190. Copyright 2018, with permission from Elsevier (ref 84). (d) Drug implant decay after different in vitro times monitored through F elemental maps. Reproduced from L. Zou, M. J. Stenslik, M. B. Giles, J. Ormes, M. Marsales, C. santos, B. Kassim, J. P. Smith, J. J. Gonzalez, X. Bu. *Journal of Analytical Atomic Spectroscopy* **1986**, *34*, 1351−1354 (ref 87), with permission from The Royal Society of Chemistry.

analysis, covering a wide range of industrial applications in which LIBS imaging can have a greater impact than single-shot LIBS. For example, Lee et al. used LIBS imaging to monitor the processing of solar cells.[73] Small maps were generated (20 × 20 pixels) with a resolution of 130 μm with a top-hat laser beam for tracking the spatial composition of Se, Cu, Ga, and In. The LIBS signal was also correlated with secondary ion mass spectrometry (SIMS). Sdvizhenskii et al. conducted an analysis of the quality and uniformity of laser cladding coatings.[74] The authors used LIBS imaging because an energy dispersive X-ray (EDX) experiment failed to measure carbon. With a spatial resolution of 40 μm, they were able to produce 3D elemental maps, with 38% of the laser spot overlapping for ablating a line and avoiding the effects of crater formation. Weiss et al. imaged fluorine with LIBS.[75] Since fluorine is difficult to detect, they opted for detecting the molecular emission of both CaF and CuF. Using a copper coating on top of the sample, the LoDs for CaF and CuF were 160 and 240 ppm, respectively. Moreover, they had to increase the laser energy by a factor of 4 (from 1.6 mJ to 6.5 mJ per pulse) to obtain the same LoD with the atomic F line at 685.6 nm. This improvement can be useful in the lime industry, in which keeping an eye on chlorine (Cl) and F concentrations is necessary. Agresti et al. already used LIBS imaging with a hand-held (HH) LIBS system for quality control in calcareous rock for the lime industry.[76] Elemental mapping was used as a support for controlling the homogeneity of the rocks, and accumulated single-shots were used on a PLS- and ANN-based model for compositional prediction.

LIBS imaging was also employed to investigate the homogeneity of lead-free piezoelectric crystal growth.[68] Maps of Ca and Zn were produced at a resolution of 12 μm, and the intensities were calibrated by EPMA. Transversal analysis of the crystal fibers showed Ca and Zn inhomogeneity, which can lead to different electrical or mechanical properties. Similar research on crystal growth has shown the segregation of Al, Sr, and Ca impurities.[77] Park et al. generated LIBS images of lithium-ion batteries (LIBs) after different laser structuring, which can increase battery capacity.[78] The lithium elemental distribution of battery electrodes, which were 140 × 200 μm in size, was shown at a resolution of 12 μm (Figure 3a). The corresponding elemental maps exhibited different lithium distributions for each pattern induced by the laser and an increase in the interfacial surface area between electrodes of up to 260%. Finally, Grünberger et al. proposed an innovative LIBS-based imaging system for analyzing polymers.[79] The laser pulse energy was drastically decreased to only produce seed electrons at the sample surface, which triggered a spark that excited the smaller ablated material. LIBS offered better sensitivity for neutral lines and molecular emission, but laser ablation-spark discharge-optical emission spectroscopy (LA-SD-OES) produced a higher ionic signal while decreasing the laser energy.

Oil Industry and Corresponding Catalysts. From the extraction process to the final sale, oil undergoes successive refining steps. Some of them include the use of aluminum-based catalysts. It is thus of prime importance to control those catalysts during the process to ensure the refining quality. Indeed, after a certain time in the oil, catalysts may be

https://doi.org/10.1021/acs.analchem.2c04910
Anal. Chem. 2023, 95, 49−69

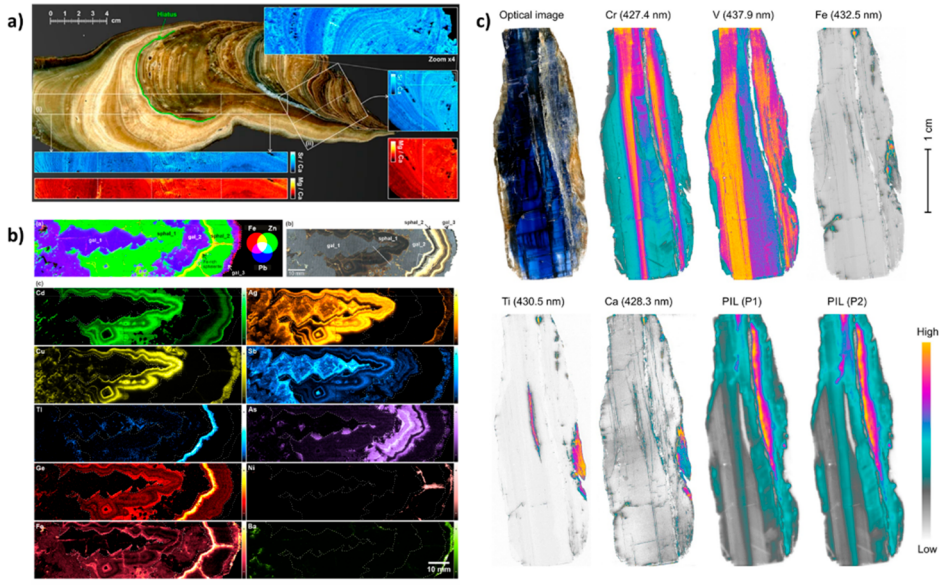

Figure 4. Geological applications of LIBS imaging. (a) Speleothem imaging of the Sr/Ca ratio (blue) and Mg/Ca ratio (red). Reprinted by permission from Macmillan Publishers Ltd.: *Scientific Reports* **2017**, *7*, 5080, Cáceres, J. O.; Pelascini, F.; Motto-Ros, V.; Moncayo, S.; Trichard, F.; Panczer, G.; Marín-Roldán, A.; Cruz, J. A.; Coronado, I.; Martín-Chivelet, J. Megapixel Multi-Elemental Imaging by Laser-Induced Breakdown Spectroscopy, a Technology with Considerable Potential for Paleoclimate Studies (ref 7). Copyright 2017. (b) Various elemental maps from different elements of Zn−Pb ore. Reprinted with permission from *Geol. Belg.* **2021**, *24*, 125−136, Baele, J.-M.; Bouzahzah, H.; Papier, S.; Decrée, S.; Verheyden, S.; Burlet, C.; Pirard, E.; Franceschi, G.; Dejonghe, L. Trace-Element Imaging at Macroscopic Scale in a Belgian Sphalerite-Galena Ore Using Laser-Induced Breakdown Spectroscopy (LIBS) (ref 102). (c) Elemental and plasma-induced luminescence maps from a blue kyanite crystal. Reprinted from *Analytica Chimica Acta*, Vol 1192, A. Nardecchia, A. de Juan, V. Motto-Ros, M. Gaft, L. Duponchel. Data fusion of LIBS and PIL hyperspectral imaging: Understanding the luminescence phenomenon of a complex mineral sample, 339368. Copyright 2021, with permission from Elsevier (ref 107).

deactivated due to external contamination, mainly from carbon. To quantify this impregnation, the selected technique should cover a large dynamic range of carbon concentrations, from ppm to tens of % mass, which perfectly aligns with the LIBS capabilities. In a recent study, Jolivet et al. monitored the carbon concentration in freshly impregnated catalysts at different times, from 30 min to 6 weeks.[80] Quantitative LIBS imaging was performed with a resolution of 25 μm to observe the dynamics of C absorption inside the catalysts, with an LoD of 305 ppm. In another study, Trichard et al. used the same setup and produced quantified images of trace metal impurities in the same kind of catalysts for V, Ni, and S in addition to C,[81] as shown in Figure 3b. Finally, the same group monitored catalyst maturation processes to understand and optimize their activation kinetics.[82]

Nuclear Applications. Following the general movement toward green energy production, the nuclear industry is currently pushing the development of next-generation fission cores and the first fusion core prototypes. In the latter case, the core environment is drastically different from the fission one: hot plasma has to be maintained to produce energy. This plasma can corrupt the surrounding walls inside the core by corrosion and/or erosion. Thus, there is a need for a technique that can remotely characterize the integrity of these walls. LIBS showed great promise for this specific application with an adapted setup and protocol. For example, the wall surface can be regarded as some number of square meters, so the resolution should be lower for meaningful sampling. In addition, picosecond lasers can be used to control the ablation rate at the lowest value possible. Two articles were published using these specific setups. In the first one, elemental and quantified erosion images were produced with a spatial resolution of 5 mm from typical graphite tiles used in reactors after being exposed to He/H plasma.[83] These 2D images corresponded to one direction and depth analysis. 200 shots were produced for the depth, resulting in images in the range of 0 to 350 mm in the poloidal coordinates and down to several μm in depth. The second article used the same experimental conditions, except that the authors produced a 3D image by adding a toroidal component and thus were able to quantify the erosion degree in a 3D map with dimensions of 7 cm × 5 cm × 4 μm[84] (Figure 3c). Finally, Choi et al. detected radioactive hotspots in nuclear power plants by conducting an isotopic analysis of iron in structural material from the nuclear core.[85] By using double-pulse LIBS with a 355 nm wavelength for ablation and 1064 nm for reheating, the authors were able to distinguish ^{54}FeO molecular emission from ^{56}FeO molecular emission and even produced an isotopic map with a resolution of 500 μm, showing the potential for double-pulse LIBS imaging for nuclear materials.

Pharmaceutical Industry. Despite being a robust analytical tool, LIBS imaging is rarely used for pharmaceutical studies. Pharmaceutical companies have to test the efficiency and purity of drugs. In addition, public health organizations can provide analysis on drugs or for hazardous element detection. In this regard, Zou et al. performed 3D elemental imaging on drug tablet coatings with a resolution of 50 μm.[86] The image depth was produced by using 30 pulses at each location on the map. In this work, the authors characterized the thickness and uniformity of tablet coatings, which play key roles in drug kinetics. The same team conducted LIBS imaging on an injectable implant for monitoring drug release by looking at the fluorine (F) line at 685.6 nm.[87] With a lateral resolution of 35

https://doi.org/10.1021/acs.analchem.2c04910
Anal. Chem. 2023, 95, 49−69

μm, they were able to track implant life-duration as illustrated in Figure 3d.

Geology. In recent years, geologists and geochemists have shown increasing interest in LIBS imaging. Compared to those of the usual techniques, either the sensitivity, resolution, and/or speed of analysis were improved.[24,88−90] In this section, trending applications of LIBS imaging for geological sample characterization are presented.

Paleo-climate. Speleothems and ice cores are paleo-climate archives. Paleo-temperature is able to be studied either by analyzing the oxygen isotopic ratios of ice cores[91] or some elemental ratios of speleothems.[92] In the latter case, LIBS images were produced directly on site[23] and in the laboratory.[7,34] The corresponding micrometric lateral resolution, down to 10 μm, allows distinguishing speleothem laminae growth, leading to the possible determination of biennial temperatures for large eras (Figure 4a). The same type of information was also obtained by analyzing marine mollusk shells, with a resolution of 100 μm.[93]

Strategic Elements. To achieve the Climate Neutrality Objectives, several countries and supra-national entities (such as the European Union) aim to reduce the transport sector's contribution to greenhouse gas emissions. In particular, moving toward zero-emission vehicles will be a crucial point of this strategy. To achieve this transition, a sufficient amount of lithium must be extracted to produce enough batteries, and lithium production is expected to grow by a factor of 5 in less than 10 years according to the World Economic Forum (WEF). Thus, there is a crucial need for a technique capable of identifying lithium in ore or directly at the mining site. Recently, we have witnessed an improvement in LIBS imaging both in laboratories and directly on-site with handled instruments, which can be regarded as the two processes of mine settlement. First, different locations are prospected, and mineral cores are extracted and sent to laboratories for analysis. Preconstructed setups can provide sensitive results in the range of ppm, with a resolution ranging from 40 to 200 μm according to the core size, at a high speed of analysis.[29] The major strengths of such setups from Elemission are the speed of analysis and the ability to conduct scanning directly on the drill core. In complement, additional strategic elements can be detected almost automatically by using semisupervised algorithms.[94,95]

Once the location of the mining site has been determined from the laboratory analysis, portable LIBS instruments can be used directly on site to guide the mining expansion.[96,97] Even though the sensitivity and resolution of such handled instruments are limited, they provide fast results that can strongly affect mining extraction efficiency. Indeed, lithium is not the only critical, strategic, or precious element. As an example, LIBS imaging has been used to produce 3D images of gold ore with a kHz frequency rate, resulting in an $8 \times 6 \times 1$ mm^3 map obtained in 20 min of analysis.[98] LIBS imaging can also identify gold veins in ore at kHz speed,[30] quantify hydrocarbons in petroleum-rich samples,[99] or even detect and identify Pt and Pd in ore extremely quickly,[100] leading to a more efficient mining extraction process. In addition, several applications and industries require rare earth elements (REEs) or rare metals. Such elements can be challenging to detect in the ppm range, even if, in some cases, LIBS alone can detect the elements of interest. In a study from Fabre et al., megapixel elemental maps with a spatial resolution of 15 μm of more than 20 elements were produced, most with a sensitivity close to the ppm level.[101]

In another study, Baele et al. successfully correlated EDS quantitative measurements with LIBS imaging signals for 8 elements, including As and Sb,[102] as shown in Figure 4b. However, quantification appears challenging when no standards are available, as external methods may not be sensitive enough for some elements. Some methods have been proposed by combining LIBS imaging and innovative data processing to achieve an accurate phase distinction inside a mineral sample to efficiently identify and quantify elements of interest. As an example, k-mean clustering has been successfully applied, combined with spatial raster analysis, for the detection of La.[103] Another way to solve this issue is to combine several detection approaches. An easy method might be to adjust the temporal acquisition of the signal for detecting molecular emission or plasma-induced luminescence (PIL). In this regard, the combination of typical LIBS imaging for atomic and molecular emission, as well as luminescence, allowed easy imaging of elements such as Eu, Gd, or Sm,[104] with extremely competitive LoDs of 10, 40, and 40 ppm, respectively. Finally, we present the possibilities offered by combining two different but complementary techniques: LA-ICP−MS and LIBS imaging of uranium ore.[105] Briefly, LIBS was used to perform a rough and rapid scan to map the total area. Then, LA-ICP−MS was used in specific and restricted areas where U was detected. LA-ICP−MS is typically more sensitive than LIBS and provides isotopic information; however, it is used for imaging only smaller regions.

Fundamental Applications. Aside from specific geological applications, LIBS imaging can also offer solutions to more fundamental issues. Several minerals produce very complex and heterogeneous samples, and phase discrimination and classification can be challenging because different phases can have the same elemental compositions but at different concentration ratios. Zivkovic et al. used an unsupervised clustering algorithm combined with CF-LIBS for an accurate classification of the different phases in an archeological mortar.[106] In another study from Cugerone et al., a combination of LA-ICP−MS, electron backscattered diffraction (EBSD), and LIBS imaging was employed for sphalerites, a typical rock mineral that contains rare metals (Ge, Ga, In, and Cd).[70] By combining all the information from the different techniques, the elemental behavior and distributions were correlated with the geographical location of the minerals, which may provide significant insight into how the rock is formed. The same group of authors had already conducted a prospective work on this topic by studying the Ge distribution of sphalerite with coupled LIBS imaging and EBSD.[69] On the other hand, from a totally different perspective, Nardecchia et al. combined PIL and LIBS imaging to study a kyanite crystal[107] (Figure 4c). The PIL signal in imaging mode can be complex, and due to its long emission, two successive signals might overlap. The aim of this work was to use LIBS imaging data to scale PIL data by compressing and fusing both data types, opening the way for fusing data between LIBS and other techniques.

Forensic Applications. Due to its fast use and sensitivity in the ppm range for most elements, LIBS is already employed in forensic applications, such as determining gunshot residues (GSRs)[108] or in various other forensic situations in its single-shot modality.[109] LIBS imaging is currently being evaluated for the same GSR analysis as well as for shooting distance

https://doi.org/10.1021/acs.analchem.2c04910
Anal. Chem. 2023, 95, 49−69

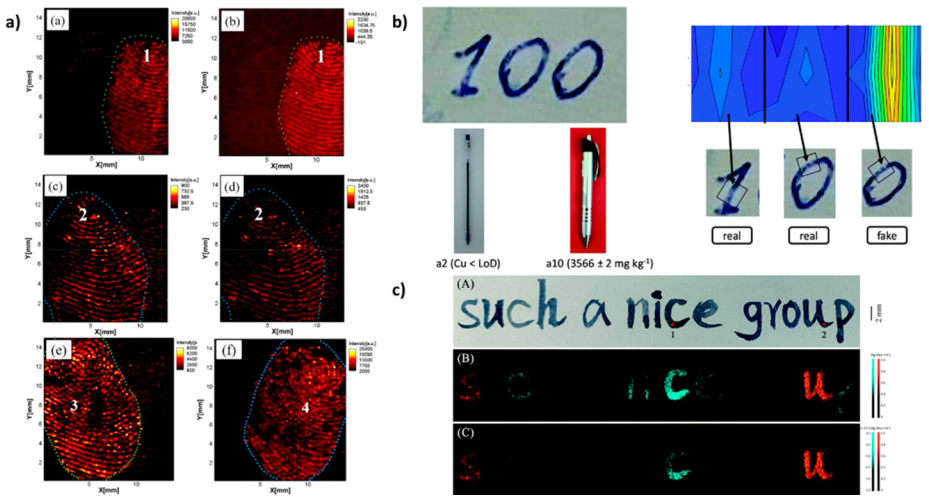

Figure 5. Forensic applications of LIBS imaging. (a) Elemental images of overlapping fingerprints for different elements. Reprinted from Spectrochimica Acta Part B: Atomic Spectroscopy, Vol 134, J-H. Yang, S-J. Choi, J. J. Yoh, Toward reconstruction of overlapping fingerprints using plasma spectroscopy, pp. 25−32. Copyright (2017), with permission from Elsevier (ref 112). (b) PCA maps based on LIBS imaging highlighting which number was added. Reproduced from Hilario, F. F.; Lime de Mello, M.; Pereira-Filho, E. R. *Analytical Methods* **2009**, *13*, 232−241 (ref 114), with permission from The Royal Society of Chemistry. (c) Elemental images of handwritten documents using different inks. Reproduced from P. Yin, E. Yang, Y. Chen, Z. Peng, D. Li, Y. Duanb, Q. Lin. *Chemical Communications* **2021**, *57*, 7312−7315 (ref 115), with permission from The Royal Society of Chemistry.

determination.[54] In studies from both Vander Pyl et al. and Lopez et al., LIBS imaging was applied to targets after shooting from different distances.[54,110] By looking at the Ba and Pb elemental distributions, the authors demonstrated that the elemental pattern distribution depends on the shooting distance, and it may be possible to estimate the shooting distance from LIBS imaging. With the rapid development and affordability of LIBS imaging setups, new applications related to the forensic field are starting to appear. These "exotic" applications show promising results, which might cause forensic applications of LIBS imaging to increase in the future. Rather than a complete review in this field, which is available elsewhere,[111] we will present a subjective selection of research articles in which LIBS imaging was demonstrated to hold great promise for forensic studies.

Yang et al. were able to differentiate fingerprints from two different people using single-shot LIBS and principal component analysis (PCA).[112] LIBS imaging was employed with a lateral resolution of 125 μm to reconstruct each fingerprint in an overlap situation, as illustrated in Figure 5a. The same research group published a similar work, in which the aging effect was also considered using soft independent modeling of class analogy (SIMCA).[113] This breakthrough might be useful in crime investigation when fingerprints need to be analyzed: in this specific case, rapid LIBS imaging analysis can identify fingerprint authors and even deconvolute multiple overlapping fingerprints due to the specific chemical composition of each individual fingerprint. Moreover, Hilario et al. used LIBS imaging for handwritten documents.[114] By using PCA maps, two inks of the same color were tested to identify any "fake" written information added to a document (Figure 5b). Even if the difference between the writing of two pens was not visible to the naked eye, LIBS imaging produced two different PCA scores for each ink, leading to their identification. This promising application can be useful to prove the veracity of official handwritten documents. LIBS imaging was also used for steganography:[115] by using inks with different elemental compositions, Yin et al. were able to reveal hidden messages in a handwritten document, as shown in Figure 5c.

Biology and Medicine. The direct imaging of endogenous chemical elements in plants or in animal and human tissues is of paramount interest for a global description of the pathophysiological state of organs.

LIBS microscopy can be used to monitor the elemental composition of any kind of sample. In regard to studying biological or biomedical specimens, the ability to interpret 2D elemental images of chemical elements with LIBS imaging provides more information compared to the single-shot microanalysis strategy performed with LIBS or competitive technology. In fact, elemental imaging with LIBS provides researchers and clinicians with the possibility of collecting the complete spectrochemical information on the entire surface of the specimen of interest, without bias or *a priori*. This point is particularly important because biomedical specimens are highly heterogeneous in terms of cellular content. Each organism is composed of several tissues, and each tissue is made of several cell types. The cell diversity in vegetal, animal, and human tissues is incredible, as is pathophysiological cellular chemical content. As an example, in a given tissue area of a few hundred square micrometers, one can find bone tissue next to muscular cells, with surrounding epithelial cells and neighboring blood vessels containing blood cells. Except for the analysis of blood or other body fluids, the advantage of tissue elemental imaging over single-shot microanalysis is obvious in biomedicine, and we strongly encourage the LIBS community to embrace this strategy for analyzing biomedical tissues with LIBS. A few reviews have already described the relevance of LIBS imaging for biomedicine;[3−5] however, in this section, we will focus on more recent applications of label-free LIBS elemental imaging for biology and medicine, discussing how this tool is facilitating a broader understanding of the role of metals in systems biology and how environmental exposure can be monitored in plant, animal, and human pathology.

The French research group of Dr. Motto-Ros historically took the initiative in the development and improvement of the

https://doi.org/10.1021/acs.analchem.2c04910
Anal. Chem. 2023, 95, 49−69

LIBS technique for bioimaging the elemental content of animal organs.[19] A cornerstone study reported the ability to use ultraviolet-based LIBS imaging to study the distribution of gadolinium−silicon-based nanoparticles in a multielemental and quantitative manner.[6] The elemental analysis was performed in murine epoxy-embedded kidneys collected at different time points after intravenous injections (Figure 6a), and an image resolution of 40 μm was achieved.

The same team subsequently switched to an infrared laser source to image in 3D the same small theranostic nanocompounds in kidneys and at the whole-organ scale (Figure 6b). They successfully managed to improve the accessible resolution as low as ∼10 μm in all 3 dimensions.[66] They logically further developed their expertise to focus on the imaging of human specimens. They obtained the proof-of-concept for mastering the ablation process for the 2D-LIBS multielemental analysis of soft matrices, i.e., human paraffin-embedded skin biopsies, generating descriptive multielemental maps of the endogenous elements distributed within normal skin and a series of skin cancers (Figure 6c).[116] Interest in the use of LIBS imaging for medicine was first demonstrated by analyzing the elemental content of abnormal histopathological features, such as pigments or vacuoles, reported in human granulomas, lymph nodes, or scar specimens. LIBS imaging provided evidence of exogenous soluble compounds, such as aluminum salts (Figure 6d), micro- or nanosized metal particles made of titanium or tungsten, and even pure copper foreign bodies.[117]

Elemental Imaging of Plants. For plants, LIBS imaging can be performed on different parts, such as the root, stem, flower, or fruit.

The collected information is useful for understanding potential nutrient dysregulations (Na, K, P, etc.) that reflect general plant health as well as diseases, insufficient nutritional intake, and even possible contamination by polluted atmosphere, water, and/or soils.[118]

With the aim of investigating the spatial control of nutrient exchange in plant rhizospheres, LIBS elemental imaging was used to image both organic content and inorganic constituents in root−rhizosphere−soil systems.[119] This study included the generation of elemental images for 17 macronutrients, micronutrients, and matrix elements from soil, with a resolution of ∼100 μm. One of the main results was the observation of fine-scale chemical gradients within small samples of ∼1 mm of switchgrass roots. This demonstrated that LIBS imaging is suitable as an effective spatially resolved technique for the sensitive and rapid elemental mapping of complex soil matrices and plant rhizospheres, with simultaneous multielement acquisition and minimal sample preparation or destruction.

LIBS elemental bioimaging was also used to measure the effects of selenium enrichment on the distribution of diffusible endogenous cations in edible *Pleurotus* mushrooms.[120] This study led to the conclusion that selenium enrichment altered the distribution of K and Mg and increased Ca bioaccumulation in the lower part of the pink oyster mushroom (*Pleurotus djamor*). From these results, it was deduced that selenium altered Ca, K, and Mg transport and compartmentalization, thus impacting global fungal metabolism.

Because of its ability to analyze lightweight elements, LIBS imaging was advantageously chosen to analyze the presence of lithium in the leaves of *Podocarpus macrophyllus*.[121] Similarly,

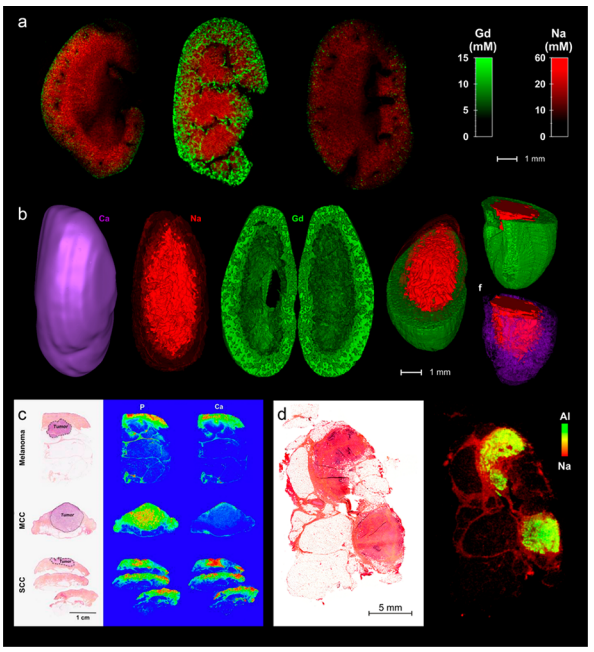

Figure 6. Historical milestones in LIBS imaging for biomedical applications. (a) Distribution of gadolinium-based nanoparticles in the kidney as a function of the time elapsed after administration. Quantitative imaging of Gd (green) and Na (red) in coronal kidney sections. The images were recorded at a 40 μm resolution and represent 30,000 pixels. Reprinted by permission from Macmillan Publishers Ltd.: *Scientific Reports*, Laser spectrometry for multi-elemental imaging of biological tissues. Sancey, L.; Motto-Ros, V.; Busser, B.; Kotb, S.; Benoit, J. M.; Piednoir, A.; Lux, F.; Tillement, O.; Panczer, G.; Yu, J. *Sci. Rep.* **2014**, *4*, 6065 (ref 6). Copyright 2014. (b) 3D imaging at the whole-kidney scale. Ca (violet), Na (red), and Gd (green) are shown. Right part: Kidney sections allowing the observation Gd and Na combined on coronal or axial sections or with Ca. Reprinted by permission from Macmillan Publishers Ltd.: *Scientific Reports*, 3D Imaging of Nanoparticle Distribution in Biological Tissue by Laser-Induced Breakdown Spectroscopy. Gimenez, Y.; Busser, B.; Trichard, F.; Kulesza, A.; Laurent, J. M.; Zaun, V.; Lux, F.; Benoit, J. M.; Panczer, G.; Dugourd, P.; Tillement, O.; Pelascini, F.; Sancey, L.; Motto-Ros, V. *Sci. Rep.* **2016**, *6*, 29936 (ref 66). Copyright 2016. (c) Elemental imaging of different skin cancer types. Left panel: histological image of the three studied skin cancer types after hematoxylin-eosin-saffron (HES) staining (melanoma metastasis, Merkel cell carcinoma (MCC) and squamous cell carcinoma (SCC)). The different skin layers, i.e., the epidermis, dermis, and hypodermis, are visible, and the dashed line indicates the tumor region. Right panel: P and Ca elemental distributions shown with a cold-to-warm color scale. Reprinted from *Spectrochimica Acta Part B: Atomic Spectroscopy*, Vol 133, Moncayo, S.; Trichard, F.; Busser, B.; Sabatier-Vincent, M.; Pelascini, F.; Pinel, N.; Templier, I.; Charles, J.; Sancey, L.; Motto-Ros, V. Multielemental imaging of paraffin-embedded human samples by laser-induced breakdown spectroscopy, 40−44. Copyright 2017, with permission from Elsevier (ref 116). (d) Histopathological morphology of a cutaneous granuloma with corresponding elemental images obtained after LIBS (right panels). LIBS analysis revealed high levels of aluminum (Al, in green) in the immunohistiocytic areas. Sodium (Na, in red) enabled the visualization of the global tissue architecture. Reprinted by permission from Macmillan Publishers Ltd.: *Modern Pathology*, Characterization of foreign materials in paraffin-embedded pathological specimens using in situ multielemental imaging with laser spectroscopy. Busser, B.; Moncayo, S.; Trichard, F.; Bonneterre, V.; Pinel, N.; Pelascini, F.; Dugourd, P.; Coll, J. L.; D'Incan, M.; Charles, J.; Motto-Ros, V.; Sancey, L. *Mod. Pathol.* **2018**, *31*, 378−384 (ref 117). Copyright 2017.

https://doi.org/10.1021/acs.analchem.2c04910
Anal. Chem. 2023, 95, 49−69

a double-pulse strategy was employed to study the chromium distribution in rice leaves.[122]

In an attempt to improve the sensitivity and ability of detecting harmful chemicals in plants, a recent study employed a strategy based on the use of nanoparticle-enhanced laser-induced breakdown spectroscopy (NELIBS), a technique invented by the group of Prof. De Giacomo from university of Bari, Italy.[123]

The distribution of toxic agents, such as chlorpyrifos and cadmium, was analyzed in the leaves and stems of lettuce in a space-resolved manner. The main findings were that heavy metals are distributed unevenly in edible plant leaves, with higher concentrations in veins than in mesophyll. In this study, NELIBS achieved an increased sensitivity by 2 orders of magnitude compared to the standard LIBS technique.[124]

Recently, LIBS imaging was used to help describe the cadmium distribution in the white mustard crop plant (*Sinapis alba* L.).[125] The authors used a combination of LIBS imaging and micro-LIBS to achieve lateral resolutions of 100 and 25 μm, respectively. This allowed observing the spatial cadmium distribution in plant roots exposed to either $CdCl_2$ solutions or cadmium telluride quantum dots (CdTe QDs, Figure 7).

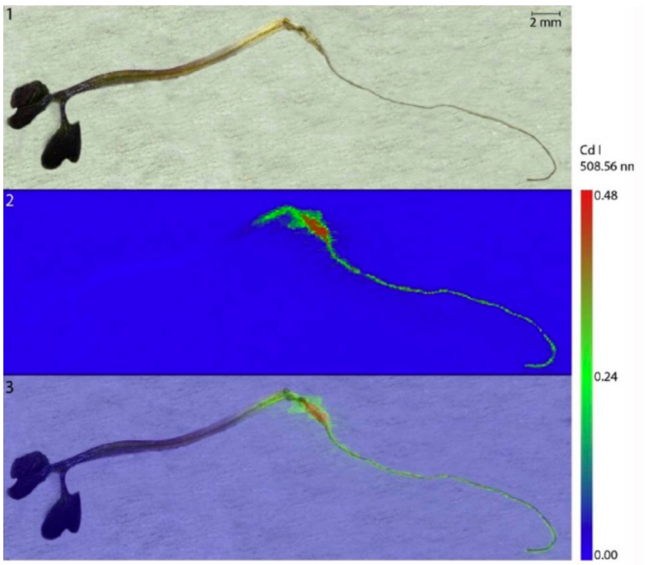

Figure 7. Example of LIBS elemental images of plants. (1) Photograph of *Sinapis alba* plants exposed to CdTe QDs before LIBS measurements. (2) LIBS elemental map constructed for the Cd I 508.56 nm emission line (spatial resolution of 100 μm). (3) Overlap of the original photograph of a plant with a LIBS map. The scale shows the total emissivity of the selected emission line. Reprinted from *Chemosphere*, Vol 251, P. Modlitbová, P. Pořízka, S. Střítežská, Š. Zezulka, M. Kummerová, K. Novotný, J. Kaiser. Detail investigation of toxicity, bioaccumulation, and translocation of Cd-based quantum dots and Cd salt in white mustard, 126174. Copyright 2020, with permission from Elsevier (ref 125).

Elemental Imaging of Animal Tissue. LIBS imaging has been used in a wide range of applications for analyzing animal tissues. Notably, it appears that this technique is well-suited for imaging the pharmacokinetics of metal-based nanoparticles and therapeutics in the organs of animals or the pathophysiological state of endogenous elements in tissues.

LIBS was notably used for imaging the distribution of ultrasmall luminescent gold (Au) particles referred to as nanoclusters (NCs).[126] In combination with X-ray fluorescence, LIBS imaging allowed the proper visualization of Au in the organs and the tumors of animals that were previously injected with Au NCs. This work is of importance since it demonstrated once again that LIBS is an easy and inexpensive method for evaluating the pharmacokinetics of metal-NPs in organisms. Here, LIBS determined a high accumulation of Au in the kidney (Figure 8a), whereas Au was barely detected in the liver and spleen. From this, it was obvious that these innovative compounds were preferentially eliminated through the urine on a very fast time scale. In complement, LIBS effectively measured the accumulation of Au-based nanocompounds in tumors that were subcutaneously grafted. This work also underlines the benefit of combining tissue-scale

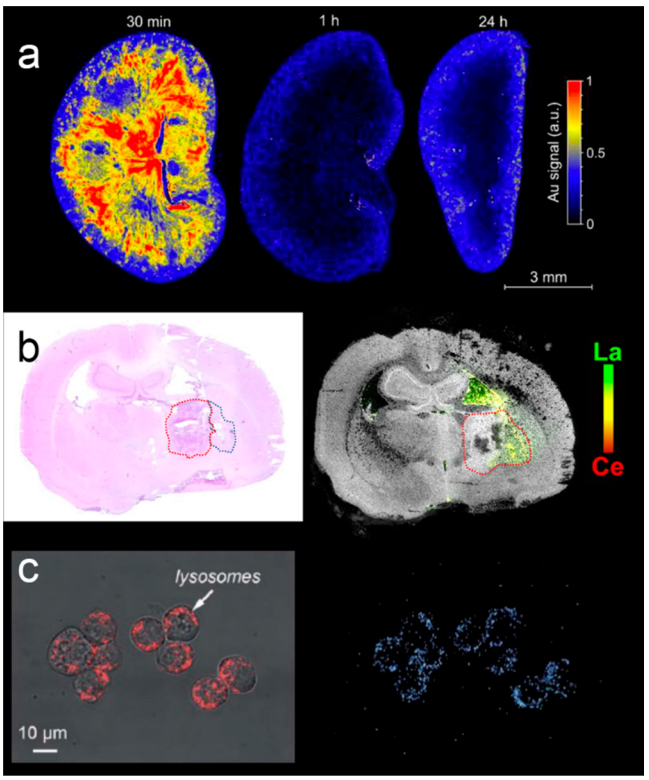

Figure 8. LIBS imaging in biological applications for animal tissues and cells. (a) Kidney slice images obtained 30 min, 1 h, and 24 h after injection of Au NPs. Reproduced from Elemental and optical imaging evaluation of zwitterionic gold nanoclusters in glioblastoma mouse models. X. Le Guével, M. Henry, V. Motto-Ros, E. Longo, M. I. Montañez, F. Pelascini, O. de La Rochefoucauld, P. Zeitoun, J.-L. Coll, V. Josserand, L. Sancey. *Nanoscale* **2018**, *10*, 18657−18664 (ref 126), with permission from The Royal Society of Chemistry. (b) Brain section with a glioma, surrounded by the red dashed line, several days after the local administration of LaCe NPs (DOI 10.1016/j.jneumeth.2022.109676). Reprinted from *Journal of Neuroscience Methods*, Vol 379, B. Busser, A-L. Bulin, V. Gardette, H. Elleaume, F. Pelascini, A. Bouron, V. Motto-Ros, L. Sancey. Visualizing the cerebral distribution of chemical elements: A challenge met with LIBS elemental imaging. 109676. Copyright 2022, with permission from Elsevier (ref 127). (c) Nanoscale LIBS imaging of InP nanoparticles within single cells. Optical image of cells stained with LysoTracker Red DND-99 (left) and LIBS imaging of In(I) at 410.2 nm (right). Reproduced from Nanoscale laser-induced breakdown spectroscopy imaging reveals chemical distribution with subcellular resolution. Y. Meng, C. Gao, Z. Lin, W. Hang, B. Huang. *Nanoscale Advances* **2020**, *2*, 3983 (ref 128), with permission from The Royal Society of Chemistry.

https://doi.org/10.1021/acs.analchem.2c04910
Anal. Chem. 2023, 95, 49−69

elemental imaging, such as LIBS, with subcellular-scale elemental imaging modalities, such as X-ray fluorescence, for collecting complementary information.

It has been established that the choice of instrumental analytical technique is crucial for imaging metal-nanocompounds in tissues.[129] In the specialized field of brain elemental imaging, almost all elemental imaging modalities have been employed for the direct imaging of diffusible ions, such as Na^+, Mg^{2+}, Ca^{2+}, K^+, and Cl^-, within brain tissue.[130] In this aforementioned article, the global landscape of techniques described for brain elemental imaging included proton-induced X-ray emission (PIXE), X-ray fluorescence microscopy (XFM), SIMS, and laser-ablation inductively coupled plasma−mass spectrometry (LA-ICP−MS). However, LIBS imaging was not included in the list despite being a method of choice for imaging brain tissues. Yet, LIBS may be very effective and helpful for researchers specializing in both nanomedicine and neurology.[127] The visualization of endogenous chemical elements, such as P, Mg, Ca, Na, Cu, and Fe, was easily achieved with LIBS. The corresponding chemical maps described the localization of these elements of interest in animal brain cryosections obtained from adults and even from mouse embryos. The ability to image and quantify zinc in the fetal brain with LIBS allowed us to study the distribution and time-course regulation of zinc during the development and maturation of cerebral structures during embryogenesis. What was shown for zinc remains true for any other endogenous chemical element, and LIBS should become one of the most reliable and user-friendly methods for evaluating the spatial and temporal regulation of metal homeostasis at the whole-organ scale. In a different study, LIBS was also used to image Ca, Mg, Na, Cu, and P distributions in 10 mouse brain sections.[131] Here, again, LIBS demonstrated its capacity to image at the whole-organ scale, with the ability to perform 3D imaging.

Bulin et al. also used LIBS imaging as a key analytical modality to image lanthanide-cerium-based nanoscintillators.[132] These LaF_3:Ce nanocompounds were imaged in rat brains bearing orthotopic glioblastomas. In fact, the presence of both La and Ce at the site of the tumors (Figure 8b) indicated a positive response to radiotherapy, as well as the good stability of the nanoscintillators *in situ*. Therefore, this study was the first to show that LIBS imaging is beneficial for indirectly reflecting the efficacy of an anticancer treatment.

To keep up with radiotherapy improvements, LIBS imaging was also successfully used to establish that boron-containing fluorophores effectively reached tumors in a tumor-bearing chicken embryo model.[133] In the context of boron neutron capture therapy (BNCT, an innovative radiotherapeutic modality based on neutrons), boron imaging truly represents one of the most promising application fields for LIBS, since this element is a very light chemical element and is therefore difficult to image with other elemental imaging modalities.

One of the most remarkable steps forward in the bioimaging of metal-NPs was the reporting of the intracellular localization of indium-based NPs with double-pulse LIBS technology.[128] This was the first time that a LIBS imaging instrumentation setup successfully managed to surpass micrometer resolution for a biological sample (Figure 8c). In this study, Meng et al. used a nanolaser probe to improve the lateral resolution down to 500 nm. The combination of a femtosecond laser (515 nm for sampling) with a nanosecond laser (266 nm for emission enhancement) allowed the visualization of metal-NPs within single cells. Additionally, the indium elemental images exquisitely corresponded with the fluorescence images of lysosomes in cells, suggesting that these NPs enter the cells through endocytosis before being trapped in lysosomes. Not only did this inspirational study provide the first images of the subcellular distribution of metal-NPs in organelles with LIBS, but with an absolute LoD of 18.3 fg, it paved the way for exciting functional studies about the behaviors of and interactions between metal-NPs and cells.

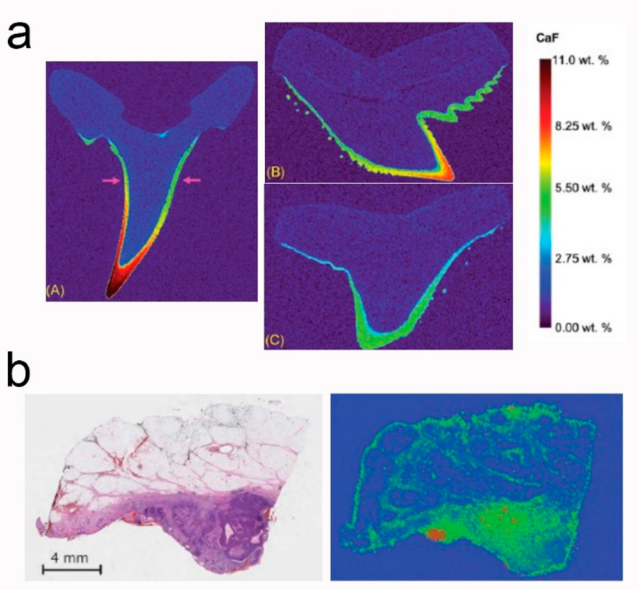

Figure 9. LIBS molecular imaging of shark teeth and LIBS elemental imaging in human skin tissues embedded in paraffin. (a) CaF distribution in the teeth of the (A) sand tiger shark (with the cross-section location indicated by the red dashed line), (B) tiger shark, and (C) hammerhead shark using the 50 μm spot method. Reproduced from Determination of Fluorine Distribution in Shark Teeth by Laser-Induced Breakdown Spectroscopy. Manard, B. T.; Hintz, C. J.; Quarles, C. D.; Burns, W.; Zirakparvar, N. A.; Dunlap, D. R.; Beiswenger, T.; Cruz-Uribe, A. M.; Petrus, J. A.; Hexel, C. R. *Metallomics* **2022**, *14*, mfac050 (ref 134), with permission of Oxford University Press, CC BY license. (b) Analysis of a basal-cell carcinoma: histological image (left) and Ca intensity map obtained with LIBS. Reproduced from Imaging margins of skin tumors using laser-induced breakdown spectroscopy and machine learning. K. Kiss, A. Sindelarova, L. Krbal, V. Stejskal, K. Mrazova, J. Vrabel, M. Kaska, P. Modlitbova, P. Porizka, J. Kaiser. *Journal of Analytical Atomic Spectroscopy* **2021**, *36*, 909 (ref 137), with permission from The Royal Society of Chemistry.

In a study conducted on shark teeth (Figure 9a), fluorine imaging was performed through the spectral emission lines of the calcium fluorine (CaF) molecule.[134] The strategy to indirectly analyze the distribution of an element via the use of molecular emission from plasma is very relevant and contradictory to the general dogma claiming that LIBS is efficient for analyzing chemical elements alone, without knowledge about the molecular information. The application of molecular emissions in LIBS is indeed a growing area of research,[135] and we believe that there are many benefits to developing innovative LIBS imaging projects that also include molecular emission analysis. Recently, both elemental and molecular emissions were studied within a single project aiming at studying cancer in an animal model.[136] In this work,

https://doi.org/10.1021/acs.analchem.2c04910
Anal. Chem. 2023, 95, 49−69

melanoma cells were xenografted subcutaneously in mice. Once the tumors were excised, they were prepared for LIBS analysis, and the K elemental emission signals and CN molecular emission signal were selected for an algorithm-based discrimination between the melanoma and the surrounding nonmalignant dermis.

Elemental Imaging of Human Tissue. The elemental analysis of human tissue is still a neglected area of research, especially because of the legislation and mandatory administrative procedures intrinsically linked to medical research involving human subjects, as defined by the Helsinki declaration from the World Medical Association.[138] We must emphasize that every research protocol aiming at analyzing any kind of human fluid or human tissue is considered medical research, and investigators must conform to the Helsinki declaration by providing the ethics committee's approval number, as well as information regarding the written informed consent from patients. Several laboratories have developed projects aimed at improving cancer diagnosis, which is the most studied human pathology with LIBS. Most of these studies are performed with LIBS in a microanalytical setting, either on fluids (blood or serum) or tissues.[139] We believe that spatial information is an important parameter, especially for studying solid cancer diseases in which tumor heterogeneity is key. Accordingly, we strongly encourage research teams to study solid malignancies with LIBS instruments tuned for elemental imaging, since the 2D spatial capability reflects the heterogeneous signals of tumors within their native environment. In a seminal work, Moncayo et al. studied the distribution of endogenous chemical elements (Na, P, Ca, Fe, Mg, and Zn) in normal human skin, as well as in several different skin cancer types, such as malignant melanoma, squamous cell carcinoma, and Merkel cell carcinoma.[116] This descriptive approach allowed the obtainment of monoelemental images from human diseases, with a modest capacity to investigate differences between the elemental maps of normal versus cancer skin regions. In accordance with this work, another small series of human skin tissues was recently imaged with LIBS, and the distribution of several elements of interest (Na, K, Mg, and Ca) was studied in a malignant melanoma, squamous cell carcinoma, basal cell carcinoma (Figure 9b), and hemangioma.[137] This work also included the use of a self-organizing map (SOM) algorithm for clustering pixels according to elemental information. Another work aimed at studying the elemental distribution of elements (Ca, Mg, Na, C, Al, Fe, Si, and Cu) as well as molecular fragments (CN and C_2) in human lung specimens used a k-means algorithm to classify the elemental information on each pixel.[140]

Notably, the first multicenter clinical trial with LIBS imaging has been registered.[141] This ongoing retrospective study aims to recruit 100 participating patients with lung diseases. The overall goal of this MEDICO-LIBS clinical study is to evaluate the feasibility of using LIBS imaging to identify, localize, and possibly quantify metals within selected human specimens with idiopathic lung diseases. This study will generate massive databases that will necessitate the use of chemometric toolboxes to fully utilize the multidimensionality of the spectral information combined with the medico-biological information.

We believe that the use of chemometrics for treating such large data sets is key (please refer to the next paragraph) and will undeniably play a major future role in the LIBS imaging of human tissues. In addition, we anticipate great collaborations between LIBS imaging physicists and medical investigators. The former are in charge of developing instruments to image/quantify endogenous and exogenous elements with increased (nanoscale) resolution, and the latter are in charge of compliance with the ethical guidelines for medical research as well as for the choice of relevant specimens.

Regarding the different biomedical LIBS elemental imaging studies recently published, all studies focused on the semiquantitative information contained intrinsically in elemental images, and no absolute quantitative studies were performed. Several difficulties for calibration remain,[142] and we believe that the absolute concentrations of elements at the pixel level are not yet necessary for the proper clinical interpretation of elemental images. However, recent developments in calibration-free LIBS microanalysis[143] could lead to possible LIBS imaging applications, and we greatly encourage the scientific community to work on this promising challenge.

PROCESSING AND CHEMOMETRICS IN LIBS IMAGING

To better understand the role of chemometrics in LIBS imaging today and to understand how it could evolve in the years to come, it is important to review the history of this spectroscopic imaging technique. Even if LIBS spectroscopy was, at the beginning, a technique for physicists who developed spectroscopic measurement systems, this technique has become a real analytical chemistry technique. Nevertheless, from our point of view, it is still not well-known in the field, hence the need for this article. Similar to many other spectroscopic techniques, LIBS spectroscopy was first used for bulk analysis to investigate the presence of specific elements in complex samples. It has made its way into the industrial world for material characterization and has also become one of the flagship spectroscopic techniques in scientific research, having been installed on the Martian exploration rovers.

Hyperspectral LIBS imaging dates back to the 2000s, having exceptionally evolved and continuing to receive growing interest from all scientific communities, as this spectroscopic imaging technique has many interesting features. We will briefly discuss them here. First, this technique has a very high dynamic range allowing the detection of almost all elements from the percent to the ppm scale. It is also very fast with today's kHz acquisitions; that is, it can acquire 1000 spectra per second with a spatial resolution of approximately 10 μm. In the 2000s, LIBS imaging data sets contained approximately 1000 pixels (i.e., 1000 spectra); they can now contain more than 10 million pixels, acquired in a few hours, for a sample exploration at the micrometer scale on a surface of several cm^2. Each of these spectra is often made up of several thousand wavelengths; such a data set acquired on a sample exceeds several gigabytes of computer memory. As the LIBS spectrum presents fine and numerous emission lines, the researchers first generate a map of a given element by a simple integration of the signal measured at a supposedly specific wavelength of the element in question. It is the most commonly used method for many spectroscopic imaging techniques. Indeed, it is a simple and fast approach for generating elemental images from LIBS spectra, and it is quite natural that we continue to use it. We will see later in this section that researchers are still trying to improve this univariate use of data to better respond to the constraints and specificities of LIBS imaging. Nevertheless, we must not forget that the specificity of a chosen wavelength for a given element is a strong assumption. Indeed, even if a particularly thin emission line is chosen for the signal

https://doi.org/10.1021/acs.analchem.2c04910
Anal. Chem. 2023, 95, 49−69

integration, the presence of many elements in the sample (some of them unexpected) each having a large number of emission lines considerably increases the chances of an interference phenomenon. This results in overestimating the quantities of the element of interest for some spectra of the data set and ultimately in biased distribution maps. Another aspect that may appear trivial, but which is of great importance in the exploration of spectral data, is that such a univariate methodology never produces maps for unexpected elements. In a way, we can even say that we ultimately exploit only a part of the information hidden in this data set by generating chemical maps of preselected elements. We are not saying here that we should abandon this univariate approach of signal integration for generating chemical images. However, it is in our best interest to also use multivariate tools from chemometrics, which are able to simultaneously exploit the signal coming from all wavelengths of the spectral domain. We can thus attain a different and unbiased point of view of our spectral data. Above all, we have the possibility of extracting even more chemical information for an even more exhaustive exploitation and exploration of spectral imaging data. Nevertheless, we should not oppose the classical signal integration approach and multivariate chemometric methods because in fact, there are no incorrect approaches but rather incorrect interpretations of the results. It is therefore appropriate to use both techniques for LIBS imaging. The following paragraphs give an overview of the spectral data processing developed for LIBS imaging and the associated chemometric tools. We will therefore naturally exclude the works that used imaging instrumentation to acquire a large number of spectra, which were ultimately exploited in the form of a mean spectrum for bulk analysis, on a surface of interest.

First, regarding the classical integration method, the simplicity of this approach should not make us forget that precautions must be taken because it is not a push-button method. Motto-Ros et al.[144] proposed the statistical evaluation of three different signal integration methods to generate chemical images. They demonstrated that the values extracted by these different methods can generate very different maps while highlighting the most efficient map. More interestingly, the selected methodology allows the association of an uncertainty map to a generated elemental map. Therefore, it allows the evaluation of the veracity of the concentrations displayed for each pixel. Jolivet et al.[80] also used this approach to generate quantitative images of carbon in heterogeneous refining catalysts. Moreover, these images were used to estimate the LoD in this single-shot configuration, which is a very original concept.

If we return to a more general point of view, the heterogeneous character of the samples analyzed in LIBS imaging coupled with its great dynamics and good sensitivity often causes the saturation of certain emission bands in the acquired data sets. A saturation is a form of distortion that limits the signal once it exceeds a threshold. As a consequence, saturated bands with their characteristic plateaus present numerical values that do not correspond to the analytical reality of the analyzed sample. Any direct use of such data therefore leads to biased images. Unfortunately, it is not often possible to perform a second LIBS imaging experiment on the same area of a sample. The aim of a study by Nardecchia et al.[145] was to first show the importance of considering this phenomenon when analyzing spectral data at the risk of quickly creating artifacts in the generated images. Then, they proposed a method based on statistical imputation for correcting saturated bands. The concept was finally validated by considering a LIBS imaging data set of a lung biopsy. It is noted that such a spectral correction can be done within the framework of the classical integration method but also prior to a chemometric method that we will introduce later. Let us now return in a general way to an elemental image obtained by the integration method. During a LIBS imaging experiment, we systematically acquire the spectra following a grid, and the area covered by the sample is often represented by a rectangle. We have seen that the integration method allowed us to obtain a value per position of spectral measurement that corresponded *in fine* to a colored pixel in the final map. Unfortunately, all these values are not significant from an analytical and statistical point of view, although they have been calculated. Richiero et al.[146] proposed a mask strategy to locate the pixels that should be kept in the image. This concept has been applied to the characterization of archeological mortar. Additionally, the authors used image analysis tools to estimate the granulometry and the circularity of the aggregates from generated LIBS images. In the same perspective of LIBS image enhancement, Gimenez et al.[66] proposed a 3D image rendering method for better observing nanoparticle distributions in biological tissue.

Chemometrics offers many multivariate data analysis tools that have been used for a long time for other spectroscopic imaging techniques. It is therefore natural that the LIBS imaging community is interested in these tools. LIBS imaging has, however, a feature that other techniques do not have, namely, the massive nature of the acquired data set that can contain several million spectra for a single sample. Thus, chemometricians are very interested in LIBS imaging because they rarely encounter this type of massive spectroscopic data structure among the imaging techniques used in analytical chemistry. Of course, not all LIBS imaging experiments generate so many spectra, but when they do, some chemometrics algorithms must be revised to adapt to this specificity. In this case, the problem is not truly the computing capacity of our computers. We will now review all the methods in the chemometrics toolbox that have been used to enhance LIBS imaging data sets.

A hyperspectral imaging technique is primarily used to explore a partially unknown sample for which we only have the available spectra acquired over a certain region of interest. Therefore, it is quite natural that the first chemometric tools that were able to be used were unsupervised pattern recognition techniques. The best-known method in all spectroscopy fields is certainly PCA, which is the real Swiss Army knife of spectral data processing. Like all chemometrics algorithms, it is first a multivariate tool that simultaneously uses all the wavelengths of the spectral domain of interest, without any preconceived notion of the presumed importance of some of them. The analysis thus involves the extraction of principal components expressing the variances contained in the spectra. A component is analyzed in the form of a spectrum that allows the identification of different correlated or anticorrelated elements. This analysis also allows the generation of a score map associated with each component to observe the spatial distribution of the detected elements. It is a multivariate tool that is very simple to set up and use, allowing the initial chemical information on complex samples to be quickly obtained. Although it is not the subject here, it should be noted that PCA is often the core of more advanced chemometric methods. In their work, Moncayo et al.[147] used

https://doi.org/10.1021/acs.analchem.2c04910
Anal. Chem. 2023, 95, 49−69

PCA to explore a data set of more than two million spectra to characterize a complex mineral sample. They then showed how the chemical interpretation of principal components and score maps allowed the further characterization of major and minor mineral phases. This work was also an opportunity to show that such a chemometric analysis was possible considering the very large amount of data from LIBS imaging. Sirven et al.[148] have proposed a modification of this analysis called HyperPCA. It was developed with the objective of better managing particularly noisy data, which is quite common in LIBS imaging, and adapting to the sparse structure of LIBS data presenting numerous fine and often isolated lines.

The second approach, which is equally interesting in unsupervised analysis, is the so-called clustering method. Again here, we only have the spectra of the data set available, and our aim is to group all of them by similarities, i.e., include them in distinct groups of spectra called clusters. When this analysis is performed in the framework of LIBS imaging, we can create a map showing the spatial locations of these clusters in the sample region of interest. Kiss et al.[137] published a very interesting work on the application of clustering in histopathology. More precisely, a cluster analysis of LIBS imaging data sets acquired on skin samples allowed the margins of skin tumors to be defined. In other words, it was possible to highlight zones where the healthy and cancerous cells were located on the observed biological tissue without prior knowledge about it. While these clustering approaches can allow spectra to be grouped by similarity in a data set, classical algorithms, such as *k-means*, are poorly suited to detecting major compounds, minor compounds, or even traces simultaneously. In chemometrics, we say that we have an unbalanced data set because there are potentially large differences in the number of spectra between major compounds, minor compounds, and traces. Therefore, the *k-means* algorithm falls into the trap of extracting clusters that are not always representative of all the compounds present in the data set and, moreover, does not always detect the compounds present in a low number of pixels. To answer this question, Nardecchia et al.[149] proposed a new method called *embedded k-means*. These authors proposed to first apply a k-means analysis on the whole data set. The originality of this work also concerns the use of a criterion allowing the estimation of an optimal number of clusters. We must insist here on the fact that this number of clusters is always fixed *a priori*, which is not satisfactory for multivariate data exploration. As soon as this first set of clusters is fixed, a new *k-means* analysis is applied to each of the clusters containing a subset of spectra of the initial data set. The optimum number of clusters is of course obtained by using the same criterion for each of them. In this way, we can say that it is a hierarchical *k-means* analysis with an automatic choice of the optimal number of clusters. This aforementioned paper showed the potential of this approach by applying it to the exploration of a LIBS data set containing more than 2 million spectra from the analysis of a complex mineral sample. Indeed, they were able to observe both major and minor compounds as well as traces.

To conclude this section dedicated to unsupervised methods and based on the principle that exploratory methods such as PCA are poorly adapted to detect all the compounds of interest that may be present in a LIBS imaging set, we note that Wu et al.[150] developed a method called the *interesting features finder* (IFF). The objective of this approach is to detect all the compounds present in a spectral data set independently of the variance that each of them could express. It is thus possible to detect a compound regardless of whether it is major, minor, or even a trace present on a few pixels of a large LIBS data set. The authors applied this concept to the exploration of a complex sample of aerosols collected in the Arctic and demonstrated that they were able to detect some completely invisible aerosols when using a conventional exploration tool such as the PCA.

Classification (also called *supervised pattern recognition*) is the second approach in the chemometric toolbox. The goal of such an approach is to build a model capable of predicting from a spectrum its membership to a group, also referred to as a class. Classification is often more difficult to employ in spectroscopic imaging because model construction and optimization require obtaining first a training data set that will be composed of known spectrum/class pairs to establish this link. This explains the limited number of available publications on this topic (compared with those on unsupervised methods) as soon as spectroscopic imaging is considered. Here, we discuss the two main application fields of LIBS imaging today, namely, geology and biology. Regarding geology, Meima et al.[151] applied the spectral angle mapper (SAM) algorithm for the supervised classification of imaging laser-induced breakdown spectroscopy (LIBS) data to investigate variations in the chemical/mineralogical compositions of complex ore on the submillimeter to the meter scale. For their part, Müller et al.[152] used linear discriminant analysis (LDA) and semisupervised one-class support vector machines (OC-SVMs) to separate known minerals in geological drill cores based on a set of training samples while also detecting unknown material, i.e., new lithologies and/or minerals not in the training set. Regarding biology, Choi et al.[153] demonstrated that they were able to detect melanomas embedded in murine skin tissue using an SVM classification model.

The methodologies we have just discussed were, above all, qualitative, and it is quite natural that we now turn to quantitative LIBS imaging, an essential facet of analytical chemistry. We will, therefore, discuss regression methods and well-known approaches in the chemometrics toolbox. As a reminder, the aim of a regression method is to predict from a spectrum the concentration of a product of interest, and as for a classification, obtaining such a model will require first a training data set, which will be composed of known spectrum/concentration pairs to establish this link. This approach is widely used in LIBS spectroscopy for bulk analysis. However, LIBS imaging remains very anecdotal because of the difficulty of obtaining concentrations from a reference method in this specific framework. It is in the agri-food domain that we find the use of the well-known partial least-squares (PLS) regression for the estimation of quantitative maps for the analysis of beef meat[154,155] or infant formula samples.[156]

The third type of approach we can find in the chemometric toolbox is signal unmixing. This technique is particular, since it is both a qualitative and quantitative method, hence our desire to introduce it separately from the previous sections. It is indeed, first of all, an unsupervised method that works only on spectra contained in an imaging data set without any prior knowledge about them. In other words, it is potentially a good exploration technique. On the other hand, the goal of such a method is to simultaneously extract the pure spectra of all the compounds present in the data set and also give their relative concentrations within each individual spectrum. At the end of such a procedure, we obtain for each compound present in the

https://doi.org/10.1021/acs.analchem.2c04910
Anal. Chem. 2023, 95, 49−69

sample a pure spectrum used for its identification associated with its chemical distribution map. It is then possible to detect a chemical compound that is not expected and also observe its spatial distribution in the sample, which is quite a new ability compared to the abilities of other chemometric tools. The multivariate curve resolution-alternating least-squares (MCR-ALS) method is certainly the most commonly used method in chemometrics for signal unmixing. This is also the case in LIBS imaging, as shown by the work of Sandoval-Munoz et al.[157] and El Haddad et al.,[158] for the characterization of complex mineral samples. Nardecchia et al.[159] also used the MCR-ALS method to simultaneously explore two imaging data sets of the same mineral sample from LIBS and plasma-induced luminescence (PIL). This was the first time that such a data fusion approach was proposed to further the understanding of the still poorly known luminescence phenomenon of complex samples. This study was also an opportunity to propose a double data compression strategy to make MCR-ALS calculations possible for a data set of more than 2 million LIBS/PIL spectral pairs.

We will now conclude this discussion of the chemometric toolbox used in LIBS imaging by looking at neural networks, which, like the previous methods, can be used for exploration or prediction purposes. Based on the premise that nonlinear phenomena are potentially present in LIBS spectroscopic measurements, researchers have used neural networks in bulk analysis to predict concentrations from the beginning of analytical implementations. We must say that their use in the LIBS imaging field has been very limited. Thus, Pagnotta et al.[160] used self-organizing maps (SOM) for the study of ancient Roman mortars using LIBS imaging. These neural networks, also called Kohonen maps, are named after their inventor, allowing nonlinear projections of these spectral data. In this work, the generated maps were then used for clustering. In a second paper, Pagnotta et al.[161] coupled Kohonen maps with calibration-free LIBS (CF-LIBS) for the quantification on the same kind of sample. While classical neural networks (consisting of an input layer, a hidden layer, and an output layer) have never been used in LIBS imaging, the first applications of deep neural networks are appearing in the field. These networks have many layers of interconnected neurons that are particularly suitable for exploiting spatial image characteristics. The advent of such networks has of course been possible only through the development of new learning strategies as the number of parameters (i.e., weights of the neurons) for optimizing these structures has become impressive. Chen et al.[162] used a convolutional neural network (CNN) to classify rocks from elemental images that were obtained by the classical signal integration method. In consideration of the limited size of the training data set in relation to the very large number of weights of the network to be optimized, the authors have rightly proposed data augmentation strategies in order to avoid the overtraining of such a network, a situation still too often observed in many publications in analytical chemistry. This deep learning approach has also been compared to a support vector machine (SVM), another well-known nonlinear classification approach in chemometrics.

In conclusion, there are, for the moment, relatively few publications presenting the use or development of multivariate tools for the processing of spectral data from LIBS imaging experiments, contrary to other imaging techniques, such as vibrational spectroscopy. As we have already seen in this last scientific domain, and from our point of view, things will accelerate very quickly in LIBS imaging, with a significant increase in publications in the coming years. Indeed, the LIBS community is now aware of the potential of such approaches that allow us to even further investigate complex samples using a hyperspectral LIBS imaging data set in a different way. Digital pressure will also contribute to this acceleration. Indeed, today, a LIBS imaging data set acquired from a sample can contain more than 10 million spectra, and it is obvious that the integration method alone does not allow us to see below the tip of the figurative iceberg. However, we must admit that even if chemometrics has many multivariate methods in its toolbox, they are not necessarily applicable when such a large amount of data has to be considered. To respond to this new constraint, we will have to find ingenious methodologies allowing us to continue to use these tools or even to revise them completely. Finally, this evolution of chemometrics in LIBS imaging will be all the more rapid as researchers propose open-access codes and software so that we can all do our own experiments and increase our skills without having to write code, which is, of course, not necessarily our expertise.

CONCLUSION

LIBS imaging is currently strongly developing, with a significant increase in the number of articles published in recent years. Thanks to the studies carried out in the laboratory on methodological, instrumental, and applicative development, this approach is becoming progressively more mature, and it is now identified as a good candidate to become, in the near future, a reference technique for spatially resolved elemental characterization. An increasing number of companies are currently working on the development of reliable, accurate, and robust commercial instruments, gradually opening up the possibility of disseminating the technique to a larger number of users, particularly in the field of analytical sciences. As mentioned above, LIBS imaging indeed has unique features, such as a micrometer-scale resolution with detection limits down to the ppm scale, fast operating speed (up to kHz), large surface area analyzed (tens to hundreds of cm^2), and ambient operating conditions with all-optical benchtop instrumentation. To top it all off, the greatest strength of LIBS imaging is undoubtedly its ability to detect light elements with excellent sensitivities down to a hundred ppb. This makes it very complementary to more standard spectroscopic techniques, such as LA-ICP−MS and/or micro-XRF.

As we have seen in this review, LIBS imaging has many advantages that should allow it to become a full-fledged analytical technique very soon. What is certain is that at some point, its development will have to be supported by private companies. In addition, as already discussed, efforts will have to be made to facilitate the data-processing stage. The high spectral complexity, as well as the large amount of data to be processed (easily reaching one million spectra per cm^2), currently requires significant expertise to extract all the relevant information contained in the data sets. This expertise does not stop at this point because it is also necessary to detect possible measurement artifacts (self-absorption, spectral interference, etc.) at the risk of generating distribution maps not representative of the analytical reality of the sample. This aspect tends to slow down the development and diffusion of LIBS imaging as a routine technique since it remains dependent on the spectroscopic expertise of the analyst.

https://doi.org/10.1021/acs.analchem.2c04910
Anal. Chem. 2023, 95, 49−69

Aligned with this, the use of chemometric tools opens up highly relevant avenues of progress. However, these are not yet fully generalized, and research on this topic is still needed to fully understand the capabilities of these approaches. The application of new processing concepts and the management of a large volume of data allows us to imagine new analytical strategies for LIBS imaging in the short term; why not eventually use artificial intelligence for fully automated treatment? This type of tool would be perfectly adapted, even allowing real-time processing, but its implementation would require rigorous and very advanced developments.

In addition, there are other relevant aspects that would require further research. First, we can mention the detection of halogen elements that suffer from poor detectability in LIBS (LoD ∼ %). The possibility of detecting these elements indirectly through the detection of the stronger molecular emission of radicals, such as CaF or CaCl (etc.), opens up very interesting avenues.[163,164] However, to adapt this method to LIBS imaging, it is necessary to further develop strategies to ensure a reproducible and controllable formation of these radicals in plasma, compensating for the inhomogeneity of the alkaline earth elements in the samples by further developing the existing methodologies in this regard. Furthermore, and with the idea of improving the sensitivity of the technique for certain categories of elements, the use of plasma as a source of excitation for luminescence measurements seems interesting for the detection of REEs. This approach, known as plasma-induced luminescence (PIL), offers low LoDs (typically < ppm) for various REE elements, such as europium (Eu), samarium (Sm), dysprosium (Dy), gadolinium (Gd), or praseodymium (Pr), while using the same instrumentation[104,165] but covering larger delays (typically >100 μs). Finally, the analysis of complex materials (i.e., composed of several matrices) still appears challenging in terms of quantification. As discussed above, the use of complementary techniques, such as EPMA or LA-ICP−MS, allows the efficient calibration of LIBS signals. However, these approaches are time-consuming to implement, and the community needs to develop more efficient calibration methods. Further studies need to be conducted to improve the quantification capabilities of LIBS imaging, either through the development of different reference samples or through the application of methodologies, where the use of CF-LIBS and related methods represents an interesting opportunity.

AUTHOR INFORMATION

Corresponding Author

Benoit Busser − *Univ. Grenoble Alpes, Institute for Advanced Biosciences, 38000 Grenoble, France; Department of Laboratory Medicine, Grenoble Alpes University Hospital, 38000 Grenoble, France; Institut Universitaire de France, 75231 Paris, France;* orcid.org/0000-0002-9425-1577; Email: bbusser@chu-grenoble.fr

Authors

Vincent Gardette − *Université de Lyon, 69622 Villeurbanne, France*

Vincent Motto-Ros − *Université de Lyon, 69622 Villeurbanne, France*

César Alvarez-Llamas − *Université de Lyon, 69622 Villeurbanne, France*

Lucie Sancey − *Univ. Grenoble Alpes, Institute for Advanced Biosciences, 38000 Grenoble, France;* orcid.org/0000-0002-0084-3775

Ludovic Duponchel − *Univ. Lille, CNRS, Lille F-59000, France;* orcid.org/0000-0002-7206-4498

Complete contact information is available at: https://pubs.acs.org/10.1021/acs.analchem.2c04910

Notes

The authors declare no competing financial interest.

Biographies

Vincent Gardette graduated with a master's degree in Climate Science at Lyon 1 University and then obtained his PhD in Chemistry at the University of Bari in 2022. He is currently working as a Post Doc at the Light and Matter Institute (ILM) in Lyon. His research focuses on LIBS imaging applications, especially in the medical field, and also the fundamentals of laser ablation, laser−matter interactions, and plasma physics.

Vincent Motto-Ros graduated in Physics in December 2005 at University Claude Bernard Lyon 1 (Lyon, France). After two postdoctoral positions at the Canadian Space Agency (Montréal, Quebec) and at the Liphy Laboratory (Grenoble, France), he obtained an associate professor position at the University Claude Bernard Lyon 1 in 2008. Since then, he has been working on the development of the LIBS technique at the Light and Matter Institute (ILM). He has excellent international visibility for his expertise in LIBS instrumental development, quantification, experimental training, and the elemental imaging of biological tissues. He is the author of more than 100 papers in peer-reviewed journals, with 2 patents, approximately 70 presentations at national and international conferences, and 40 invited talks/lectures at international conferences. He has more than 3800 total citations and an H-index = 39 (Google Scholar).

Dr. César Alvarez-Llamas received his BSc in Physics in 2011 and his MsC in Analytical Chemistry at University of Oviedo, Spain in 2012. He received his PhD in Physics (Hons.) in 2017 working on the laser-induced breakdown spectroscopy (LIBS) technique. As a Postdoc, he studied portable LIBS equipment at the Carnot Interdisciplinary Laboratory Burgundy (ICB), Dijon, France; the analysis of collimated nanoparticles in Commissariat à l'énergie atomique et aux énergies alternatives (CEA), Saclay, France; and the use of LIBS together with acoustic signals for Mars geo-exploration applications under the NASA Mars 2020 mission in UMALASERLAB (Univ. of Málaga, Spain). He is currently working on the applications of kHz LIBS at the Institute of Light and Matter (ILM), Lyon, France.

Lucie Sancey has been Director of Research of the French CNRS at the Institute for Advanced Biosciences since 2020 in Grenoble, France. Her research activities focus on the development and evaluation of innovative compounds for cancer imaging and treatment. This includes the development of nanoagents for cancer diagnosis and therapy, particularly for new multimodal optical contrast agents and new imaging techniques for biological tissues, including fluorophores for image-guided surgery. Having been a researcher at the Light and Matter Institute (ILM) in Lyon from 2012 to 2016, she contributed to the early development of LIBS for the multielemental imaging of biological tissues. She is the author of more than 90 scientific communications; she cofounded 2 start-ups and holds 2 patents. She is a board member of SFNano (the French Society of Nanomedicine), a member of the German BNCT Society (DGBNCT), a member of the French research group "Nuclear Methods and Tools against Cancer", and a member of the scientific

https://doi.org/10.1021/acs.analchem.2c04910
Anal. Chem. 2023, 95, 49−69

steering committee of the Cancéropôle Lyon Auvergne Rhône-Alpes for the thematic axis "Innovative Technology for Health".

Ludovic Duponchel defended his PhD in Physical Chemistry in 1997 at the University of Lille (France). His research was focused on the development of a portable near-infrared spectrometer for chemical analysis in the agrofood industry. During this period, he spent two years in the Horiba Jobin-Yvon Company in Paris performing instrumental and chemometrics research. He was then first recruited as an Assistant Professor at the University of Lille in 1998 and then as a Full Professor in 2008. His academic interests focus on the development of new chemometric methodologies to further explore various kinds of datasets considering different spectroscopies and instrumental configurations, particularly in the hyperspectral imaging framework. This research was performed in the LASIRE laboratory (University of Lille). He has been the Chairman of the French Chemometrics Society under the aegis of the French Statistical Society since 2013.

Benoit Busser is a senior medical biochemist at Grenoble Hospital and an Associate Professor in Biochemistry in the Faculty of Pharmacy, Grenoble Alpes University, France. He studied pharmaceutical sciences in Strasbourg and performed his residency at Grenoble, Hospital (PharmD in 2008). Additionally, he received his PhD in cellular biology and cancer sciences from Grenoble Alpes University in 2009. He was first appointed as an assistant professor in 2009 and then as an associate professor in 2012 (university-hospital dual position). He led the cancer clinical laboratory of Grenoble Hospital for 3 years, and in 2017, he joined the Light and Matter Institute (ILM) in Lyon for a 1-year research mobility dedicated to the development of the LIBS multielemental imaging of human specimens. He received the prestigious "Young Investigator Award" in 2015 from the European Society of Molecular Imaging (ESMI) and was appointed as a member of the Institut Universitaire de France (IUF) in 2021. He is now the leader of the "elemental pathology group" at the Institute for Advanced Biosciences in Grenoble, and his current research activities include (1) exploring the fate of metal nanoparticles with therapeutic interest, (2) studying anticancer drug resistance mechanisms, and (3) characterizing the endogenous or exogenous (exposure-related) elemental content of healthy/diseased tissues with LIBS.

■ ACKNOWLEDGMENTS

This work was partially supported by the French region Auvergne Rhône-Alpes (Optolyse, CPER2016) and two French ANR grants (ANR-17-CE18-0028 "MEDI-LIBS" and ANR-20-CE17-0021 "dIAg-EM"). In addition, we gratefully acknowledge Dr. Frédéric Pelascini from Cétim Grand Est, Dr. Florian Trichard from Ablatom SAS, and Dr. Sylvain Hermelin and Professor Christophe Dujardin from the Light and Matter Institute (ILM) for fruitful discussions. We acknowledge the professional manuscript services of Springer Nature Author Services.

■ REFERENCES

(1) Piñon, V.; Mateo, M. P.; Nicolas, G. *Appl. Spectrosc. Rev.* **2013**, *48* (5), 357−383.
(2) Jolivet, L.; Leprince, M.; Moncayo, S.; Sorbier, L.; Lienemann, C.-P.; Motto-Ros, V. *Spectrochim. Acta Part B At. Spectrosc.* **2019**, *151*, 41−53.
(3) Busser, B.; Moncayo, S.; Coll, J.-L.; Sancey, L.; Motto-Ros, V. *Coord. Chem. Rev.* **2018**, *358*, 70−79.
(4) Gaudiuso, R.; Melikechi, N.; Abdel-Salam, Z. A.; Harith, M. A.; Palleschi, V.; Motto-Ros, V.; Busser, B. *Spectrochim. Acta Part B At. Spectrosc.* **2019**, *152*, 123−148.
(5) Limbeck, A.; Brunnbauer, L.; Lohninger, H.; Pořízka, P.; Modlitbová, P.; Kaiser, J.; Janovszky, P.; Kéri, A.; Galbács, G. *Anal. Chim. Acta* **2021**, *1147*, 72−98.
(6) Sancey, L.; Motto-Ros, V.; Busser, B.; Kotb, S.; Benoit, J. M.; Piednoir, A.; Lux, F.; Tillement, O.; Panczer, G.; Yu, J. *Sci. Rep* **2014**, *4*, 6065.
(7) Cáceres, J. O.; Pelascini, F.; Motto-Ros, V.; Moncayo, S.; Trichard, F.; Panczer, G.; Marín-Roldán, A.; Cruz, J. A.; Coronado, I.; Martín-Chivelet, J. *Sci. Rep.* **2017**, *7* (1), 5080.
(8) Janssens, K.; De Nolf, W.; Van Der Snickt, G.; Vincze, L.; Vekemans, B.; Terzano, R.; Brenker, F. E. *TrAC Trends Anal. Chem.* **2010**, *29* (6), 464−478.
(9) Moore, K. L.; Lombi, E.; Zhao, F.-J.; Grovenor, C. R. M. *Anal. Bioanal. Chem.* **2012**, *402* (10), 3263−3273.
(10) Pozebon, D.; Scheffler, G. L.; Dressler, V. L.; Nunes, M. A. G. *J. Anal. At. Spectrom.* **2014**, *29* (12), 2204−2228.
(11) Reich, M.; Large, R.; Deditius, A. P. *Ore Geol. Rev.* **2017**, *81*, 1215−1217.
(12) Baudelet, M.; Smith, B. W. *J. Anal. At. Spectrom.* **2013**, *28* (5), 624−629.
(13) Moenke, H.; Moenke-Blankenburg, L. *Laser Micro-Spectrochemical Analysis*; Hilger: London, 1973.
(14) Menut, D.; Fichet, P.; Lacour, J.-L.; Rivoallan, A.; Mauchien, P. *Appl. Opt.* **2003**, *42*, 6063−6071.
(15) Bette, H.; Noll, R. *J. Phys. Appl. Phys.* **2004**, *37* (8), 1281.
(16) Lucena, P.; Vadillo, J. M.; Laserna, J. J. *Anal. Chem.* **1999**, *71* (19), 4385−4391.
(17) Romero, D.; Laserna, J. J. *Anal. Chem.* **1997**, *69* (15), 2871−2876.
(18) Lucena, P.; Laserna, J. J. *Spectrochim. Acta Part B At. Spectrosc.* **2001**, *56* (2), 177−185.
(19) Motto-Ros, V.; Sancey, L.; Wang, X. C.; Ma, Q. L.; Lux, F.; Bai, X. S.; Panczer, G.; Tillement, O.; Yu, J. *Spectrochim. Acta Part B At. Spectrosc.* **2013**, *87*, 168−174.
(20) Motto-Ros, V.; Sancey, L.; Ma, Q. L.; Lux, F.; Bai, X. S.; Wang, X. C.; Yu, J.; Panczer, G.; Tillement, O. *Appl. Phys. Lett.* **2012**, *101* (22), 223702.
(21) Sancey, L.; Motto-Ros, V.; Kotb, S.; Wang, X.; Lux, F.; Panczer, G.; Yu, J.; Tillement, O. *J. Vis. Exp. JoVE* **2014**, No. 88, e51353 DOI: 10.3791/51353.
(22) Moncayo, S.; Duponchel, L.; Mousavipak, N.; Panczer, G.; Trichard, F.; Bousquet, B.; Pelascini, F.; Motto-Ros, V. *J. Anal. At. Spectrom.* **2018**, *33* (2), 210−220.
(23) Bassel, L.; Motto-Ros, V.; Trichard, F.; Pelascini, F.; Ammari, F.; Chapoulie, R.; Ferrier, C.; Lacanette, D.; Bousquet, B. *Environ. Sci. Pollut. Res.* **2017**, *24* (3), 2197−2204.
(24) Fabre, C. *Spectrochim. Acta Part B At. Spectrosc.* **2020**, *166*, 105799.
(25) Motto-Ros, V.; Moncayo, S.; Fabre, C.; Busser, B. Chapter 14 - LIBS Imaging Applications. In *Laser-Induced Breakdown Spectroscopy*, 2nd ed.; Singh, J. P., Thakur, S. N., Eds.; Elsevier: Amsterdam, 2020; pp 329−346. DOI: 10.1016/B978-0-12-818829-3.00014-9.
(26) Zhao, C.; Dong, D.; Du, X.; Zheng, W. *Sensors* **2016**, *16* (10), 1764.
(27) Krajcarová, L.; Novotný, K.; Kummerová, M.; Dubová, J.; Gloser, V.; Kaiser, J. *Talanta* **2017**, *173*, 28−35.
(28) Lednev, V.; Sdvizhenskii, P.; Grishin, M.; Cheverikin, V.; Stavertiy, A.; Tretyakov, R.; Taksanc, M.; Pershin, S. *Appl. Opt.* **2017**, *56*, 9698.
(29) Rifai, K.; Constantin, M.; Yilmaz, A.; Ozcan, L.; Doucet, F.; Azami, N. *Minerals* **2022**, *12*, 253.
(30) Rifai, K.; Doucet, F.; Özcan, L.; Vidal, F. *Spectrochim. Acta Part B At. Spectrosc.* **2018**, *150*, 43−48.
(31) Rifai, K.; Özcan, L.; Doucet, F.; Vidal, F. *Spectrochim. Acta Part B At. Spectrosc.* **2020**, *165*, 105766.

(32) Rifai, K.; Michaud Paradis, M.-C.; Swierczek, Z.; Doucet, F.; Özcan, L.; Fayad, A.; Li, J.; Vidal, F. *Minerals* **2020**, *10* (10), 918.
(33) Paradis, M.-C. M.; Doucet, F. R.; Rifai, K.; Özcan, L. Ç.; Azami, N.; Vidal, F. *Minerals* **2021**, *11* (8), 859.
(34) Motto-Ros, V.; Gardette, V.; Leprince, M.; Genty, D.; Sancey, L.; Roux, S.; Busser, B.; Pelascini, F. *Spectroscopy* **2020**, *35* (2), 34−40.
(35) Bai, X.; Ma, Q.; Motto-Ros, V.; Yu, J.; Sabourdy, D.; Nguyen, L.; Jalocha, A. *J. Appl. Phys.* **2013**, *113* (1), 013304.
(36) Motto-Ros, V.; Negre, E.; Pelascini, F.; Panczer, G.; Yu, J. *Spectrochim. Acta Part B At. Spectrosc.* **2014**, *92*, 60−69.
(37) Hai, R.; Li, C.; Wang, H.; Ding, H.; Zhuo, H.; Wu, J.; Luo, G.-N. *J. Nucl. Mater.* **2013**, *438*, S1168−S1171.
(38) Li, C.; Wu, X.; Zhang, C.; Ding, H.; Hu, J.; Luo, G.-N. *J. Nucl. Mater.* **2014**, *452* (1−3), 10−15.
(39) Ahamer, C. M.; Riepl, K. M.; Huber, N.; Pedarnig, J. D. *Spectrochim. Acta Part B At. Spectrosc.* **2017**, *136*, 56−65.
(40) Wang, X.; Liang, Z.; Meng, Y.; Wang, T.; Hang, W.; Huang, B. *Spectrochim. Acta Part B At. Spectrosc.* **2018**, *141*, 1−6.
(41) Giannakaris, N.; Haider, A.; Ahamer, C. M.; Grünberger, S.; Trautner, S.; Pedarnig, J. D. *Appl. Spectrosc.* **2022**, *76* (8), 926−936.
(42) Jantzi, S. C.; Motto-Ros, V.; Trichard, F.; Markushin, Y.; Melikechi, N.; De Giacomo, A. *Spectrochim. Acta Part B At. Spectrosc.* **2016**, *115*, 52−63.
(43) Barnett, C.; Cahoon, E.; Almirall, J. R. *Spectrochim. Acta Part B At. Spectrosc.* **2008**, *63* (10), 1016−1023.
(44) Fornarini, L.; Spizzichino, V.; Colao, F.; Fantoni, R.; Lazic, V. *Anal. Bioanal. Chem.* **2006**, *385* (2), 272−280.
(45) Bueno Guerra, M. B.; Adame, A.; de Almeida, E.; Arantes de Carvalho, G. G.; Stolf Brasil, M. A.; Santos, D., Jr; Krug, F. J. *J. Anal. At. Spectrom.* **2015**, *30* (7), 1646−1654.
(46) Hou, H.; Cheng, L.; Richardson, T.; Chen, G.; Doeff, M.; Zheng, R.; Russo, R.; Zorba, V. *J. Anal. At. Spectrom.* **2015**, *30* (11), 2295−2302.
(47) Lefebvre, C.; Catalá-Espí, A.; Sobron, P.; Koujelev, A.; Léveillé, R. *Planet. Space Sci.* **2016**, *126*, 24−33.
(48) Schiavo, C.; Menichetti, L.; Grifoni, E.; Legnaioli, S.; Lorenzetti, G.; Poggialini, F.; Pagnotta, S.; Palleschi, V. *J. Instrum.* **2016**, *11* (08), C08002−C08002.
(49) Noll, R.; Bette, H.; Brysch, A.; Kraushaar, M.; Mönch, I.; Peter, L.; Sturm, V. *Spectrochim. Acta Part B At. Spectrosc.* **2001**, *56* (6), 637−649.
(50) Boué-Bigne, F. *Spectrochim. Acta Part B At. Spectrosc.* **2008**, *63* (10), 1122−1129.
(51) Boué-Bigne, F. *Spectrochim. Acta Part B At. Spectrosc.* **2014**, *96*, 21−32.
(52) Manard, B. T.; Quarles, C. D.; Wylie, E. M.; Xu, N. *J. Anal. At. Spectrom.* **2017**, *32* (9), 1680−1687.
(53) Sweetapple, M. T.; Tassios, S. *Am. Mineral.* **2015**, *100* (10), 2141−2151.
(54) López-López, M.; Alvarez-Llamas, C.; Pisonero, J.; García-Ruiz, C.; Bordel, N. *Forensic Sci. Int.* **2017**, *273*, 124−131.
(55) Rakovský, J.; Musset, O.; Buoncristiani, J.; Bichet, V.; Monna, F.; Neige, P.; Veis, P. *Spectrochim. Acta Part B At. Spectrosc.* **2012**, *74*−*75*, 57−65.
(56) Beresko, C.; Dietz, T.; Kohns, P.; Ankerhold, G. *Tm - Technol. Mess.* **2014**, *81* (11), 537−545.
(57) Gottlieb, C.; Millar, S.; Grothe, S.; Wilsch, G. *Spectrochim. Acta Part B At. Spectrosc.* **2017**, *134*, 58−68.
(58) Taleb, A.; Motto-Ros, V.; Carru, M. J.; Axente, E.; Craciun, V.; Pelascini, F.; Hermann, J. *Anal. Chim. Acta* **2021**, *1185*, 339070.
(59) Bulajic, D.; Corsi, M.; Cristoforetti, G.; Legnaioli, S.; Palleschi, V.; Salvetti, A.; Tognoni, E. *Spectrochim. Acta Part B At. Spectrosc.* **2002**, *57* (2), 339−353.
(60) Li, J.; Hao, Z.; Zhao, N.; Zhou, R.; Yi, R.; Tang, S.; Guo, L.; Li, X.; Zeng, X.; Lu, Y. *Opt. Express* **2017**, *25* (5), 4945−4951.
(61) Darwiche, S.; Benmansour, M.; Eliezer, N.; Morvan, D. *Prog. Photovolt. Res. Appl.* **2012**, *20* (4), 463−471.
(62) Quarles, C. D.; Gonzalez, J. J.; East, L. J.; Yoo, J. H.; Morey, M.; Russo, R. E. *J. Anal. At. Spectrom.* **2014**, *29* (7), 1238−1242.
(63) Syta, O.; Wagner, B.; Bulska, E.; Zielińska, D.; Żukowska, G. Z.; Gonzalez, J.; Russo, R. *Talanta* **2018**, *179*, 784−791.
(64) Cama-Moncunill, X.; Markiewicz-Keszycka, M.; Dixit, Y.; Cama-Moncunill, R.; Casado-Gavalda, M. P.; Cullen, P. J.; Sullivan, C. *Food Control* **2017**, *78*, 304−310.
(65) Alombert-Goget, G.; Trichard, F.; Li, H.; Pezzani, C.; Silvestre, M.; Barthalay, N.; Motto-Ros, V.; Lebbou, K. *Opt. Mater.* **2017**, *65*, 28−32.
(66) Gimenez, Y.; Busser, B.; Trichard, F.; Kulesza, A.; Laurent, J. M.; Zaun, V.; Lux, F.; Benoit, J. M.; Panczer, G.; Dugourd, P.; Tillement, O.; Pelascini, F.; Sancey, L.; Motto-Ros, V. *Sci. Rep* **2016**, *6*, 29936.
(67) Trichard, F.; Sorbier, L.; Moncayo, S.; Blouët, Y.; Lienemann, C.-P.; Motto-Ros, V. *Spectrochim. Acta Part B At. Spectrosc.* **2017**, *133*, 45−51.
(68) Veber, P.; Bartosiewicz, K.; Debray, J.; Alombert-Goget, G.; Benamara, O.; Motto-Ros, V.; Thi, M. P.; Borta-Boyon, A.; Cabane, H.; Lebbou, K.; Levassort, F.; Kamada, K.; Yoshikawa, A.; Maglione, M. *CrystEngComm* **2019**, *21* (25), 3844−3853.
(69) Cugerone, A.; Cenki-Tok, B.; Oliot, E.; Muñoz, M.; Barou, F.; Motto-Ros, V.; Le Goff, E. *Geology* **2020**, *48* (3), 236−241.
(70) Cugerone, A.; Cenki-Tok, B.; Muñoz, M.; Kouzmanov, K.; Oliot, E.; Motto-Ros, V.; Le Goff, E. *Miner. Deposita* **2021**, *56* (4), 685−705.
(71) Sattmann, R.; Sturm, V.; Noll, R. *J. Phys. Appl. Phys.* **1995**, *28* (10), 2181−2187.
(72) Noll, R.; Fricke-Begemann, C.; Schreckenberg, F. *Spectrochim. Acta Part B At. Spectrosc.* **2021**, *181*, 106213.
(73) Lee, S.-H.; Choi, J.-H.; In, J.-H.; Jeong, S. *Int. J. Precis. Eng. Manuf.-Green Technol.* **2019**, *6* (2), 189−196.
(74) Sdvizhenskii, P. A.; Lednev, V. N.; Grishin, M. Y.; Cheverikin, V. V.; Stavertiy, A. Y.; Tretyakov, R. S.; Asyutin, R. D.; Pershin, S. M. *J. Phys. Conf. Ser.* **2018**, *1109*, 012066.
(75) Weiss, M.; Gajarska, Z.; Lohninger, H.; Marchetti-Deschmann, M.; Ramer, G.; Lendl, B.; Limbeck, A. *Anal. Chim. Acta* **2022**, *1195*, 339422.
(76) Agresti, J.; Indelicato, C.; Perotti, M.; Moreschi, R.; Osticioli, I.; Cacciari, I.; Mencaglia, A. A.; Siano, S. *Molecules* **2022**, *27* (6), 1813.
(77) Veber, P.; Bartosiewicz, K.; Debray, J.; Pairis, S.; Motto-Ros, V.; Borta-Boyon, A.; Levassort, F.; Velazquez, M.; Vera, R.; Kamada, K.; Yoshikawa, A. *CrystEngComm* **2020**, *22* (30), 4982−4993.
(78) Park, J.; Song, H.; Jang, I.; Lee, J.; Um, J.; Bae, S.; Kim, J.; Jeong, S.; Kim, H.-J. *J. Energy Chem.* **2022**, *64*, 93−102.
(79) Grünberger, S.; Eschlböck-Fuchs, S.; Hofstadler, J.; Pissenberger, A.; Duchaczek, H.; Trautner, S.; Pedarnig, J. D. *Spectrochim. Acta Part B At. Spectrosc.* **2020**, *169*, 105884.
(80) Jolivet, L.; Motto-Ros, V.; Sorbier, L.; Sozinho, T.; Lienemann, C.-P. *J. Anal. At. Spectrom.* **2020**, *35* (5), 896−903.
(81) Trichard, F.; Gaulier, F.; Barbier, J.; Espinat, D.; Guichard, B.; Lienemann, C.-P.; Sorbier, L.; Levitz, P.; Motto-Ros, V. *J. Catal.* **2018**, *363*, 183−190.
(82) Jolivet, L.; Catita, L.; Delpoux, O.; Lienemann, C.-P.; Sorbier, L.; Motto-Ros, V. *J. Catal.* **2021**, *401*, 183−187.
(83) Zhao, D.; Yi, R.; Eksaeva, A.; Oelmann, J.; Brezinsek, S.; Sergienko, G.; Rasinski, M.; Gao, Y.; Mayer, M.; Dhard, C. P.; Naujoks, D.; Cai, L. *Nucl. Fusion* **2021**, *61* (1), 016025.
(84) Yi, R.; Zhao, D.; Oelmann, J.; Brezinsek, S.; Rasinski, M.; Mayer, M.; Prakash Dhard, C.; Naujoks, D.; Liu, L.; Qu, J. *Appl. Surf. Sci.* **2020**, *532*, 147185.
(85) Choi, S.-U.; Han, S.-C.; Lee, J.-Y.; Yun, J.-I. *J. Anal. At. Spectrom.* **2021**, *36* (6), 1287−1296.
(86) Zou, L.; Kassim, B.; Smith, J. P.; Ormes, J. D.; Liu, Y.; Tu, Q.; Bu, X. *Analyst* **2018**, *143* (20), 5000−5007.
(87) Zou, L.; Stenslik, M. J.; Giles, M. B.; Ormes, J. D.; Marsales, M.; Santos, C.; Kassim, B.; Smith, J. P.; Gonzalez, J. J.; Bu, X. *J. Anal. At. Spectrom.* **2019**, *34* (7), 1351−1354.

https://doi.org/10.1021/acs.analchem.2c04910
Anal. Chem. 2023, 95, 49−69

(88) Fabre, C.; Trebus, K.; Tarantola, A.; Cauzid, J.; Motto-Ros, V.; Voudouris, P. *Spectrochim. Acta Part B At. Spectrosc.* **2022**, *194*, 106470.
(89) Mohamed, N.; Rifai, K.; Selmani, S.; Constantin, M.; Doucet, F. R.; Özcan, L. Ç.; Sabsabi, M.; Vidal, F. *Geostand. Geoanalytical Res.* **2021**, *45* (3), 539−550.
(90) Raneri, S.; Botto, A.; Campanella, B.; Momčilović, M.; Palleschi, V.; Poggialini, F.; Sciuto, C.; Gattiglia, G.; Volpintesta, F.; Selvaraj, T.; Živković, S.; Lorenzetti, G.; Legnaioli, S. *Spectrochim. Acta Part B At. Spectrosc.* **2022**, *194*, 106482.
(91) Petit, J. R.; Jouzel, J.; Raynaud, D.; Barkov, N. I.; Barnola, J.-M.; Basile, I.; Bender, M.; Chappellaz, J.; Davis, M.; Delaygue, G.; Delmotte, M.; Kotlyakov, V. M.; Legrand, M.; Lipenkov, V. Y.; Lorius, C.; PÉpin, L.; Ritz, C.; Saltzman, E.; Stievenard, M. *Nature* **1999**, *399* (6735), 429−436.
(92) Fairchild, I. J.; Treble, P. C. *Quat. Sci. Rev.* **2009**, *28* (5−6), 449−468.
(93) Hausmann, N.; Siozos, P.; Lemonis, A.; Colonese, A. C.; Robson, H. K.; Anglos, D. *J. Anal. At. Spectrom.* **2017**, *32* (8), 1467−1472.
(94) Müller, S.; Meima, J. *Spectrochim. Acta Part B At. Spectrosc.* **2022**, *189*, 106370.
(95) Janovszky, P.; Jancsek, K.; Palásti, D. J.; Kopniczky, J.; Hopp, B.; Tóth, T. M.; Galbács, G. *J. Anal. At. Spectrom.* **2021**, *36* (4), 813−823.
(96) Lawley, C. J. M.; Somers, A. M.; Kjarsgaard, B. A. *J. Geochem. Explor.* **2021**, *222*, 106694.
(97) Wise, M. A.; Harmon, R. S.; Curry, A.; Jennings, M.; Grimac, Z.; Khashchevskaya, D. *Minerals* **2022**, *12* (1), 77.
(98) Gervais, F.; Rifai, K.; Plamondon, P.; Özcan, L.; Doucet, F.; Vidal, F. *Terra Nova* **2019**, *31* (5), 479−484.
(99) Quarles, C. D.; Miao, T.; Poirier, L.; Gonzalez, J. J.; Lopez-Linares, F. *Fuels* **2022**, *3* (2), 353−364.
(100) Rifai, K.; Ozcan, L.; Doucet, F.; Rhoderick, K.; Vidal, F. *Minerals* **2020**, *10*, 207.
(101) Fabre, C.; Devismes, D.; Moncayo, S.; Pelascini, F.; Trichard, F.; Lecomte, A.; Bousquet, B.; Cauzid, J.; Motto-Ros, V. *J. Anal. At. Spectrom.* **2018**, *33* (8), 1345−1353.
(102) Baele, J.-M.; BOUZAHZAH, H.; PAPIER, S.; Decrée, S.; Verheyden, S.; Burlet, C.; PIRARD, E.; FRANCESCHI, G.; DEJONGHE, L. *Geol. Belg.* **2021**, *24*, 125−136.
(103) Müller, S.; Meima, J. A.; Rammlmair, D. *J. Geochem. Explor.* **2021**, *221*, 106697.
(104) Gaft, M.; Raichlin, Y.; Pelascini, F.; Panzer, G.; Motto Ros, V. *Spectrochim. Acta Part B At. Spectrosc.* **2019**, *151*, 12−19.
(105) Holá, M.; Novotný, K.; Dobeš, J.; Krempl, I.; Wertich, V.; Mozola, J.; Kubeš, M.; Faltusová, V.; Leichmann, J.; Kanický, V. *Spectrochim. Acta Part B At. Spectrosc.* **2021**, *186*, 106312.
(106) Živković, S.; Botto, A.; Campanella, B.; Lezzerini, M.; Momčilović, M.; Pagnotta, S.; Palleschi, V.; Poggialini, F.; Legnaioli, S. *Spectrochim. Acta Part B At. Spectrosc.* **2021**, *181*, 106219.
(107) Nardecchia, A.; de Juan, A.; Motto-Ros, V.; Gaft, M.; Duponchel, L. *Anal. Chim. Acta* **2022**, *1192*, 339368.
(108) Trejos, T.; Vander Pyl, C.; Menking-Hoggatt, K.; Alvarado, A. L.; Arroyo, L. E. *Forensic Chem.* **2018**, *8*, 146−156.
(109) Naozuka, J.; Oliveira, A. P. Chapter 4: Laser-Induced Breakdown Spectroscopy (LIBS) in Forensic Sensing. In *Forensic Analytical Methods*; The Royal Society of Chemistry, 2019; pp 48−78. DOI: 10.1039/9781788016117-00048.
(110) Pyl, C. V.; Ovide, O.; Ho, M.; Yuksel, B.; Trejos, T. *Spectrochim. Acta Part B At. Spectrosc.* **2019**, *152*, 93−101.
(111) Mistek, E.; Fikiet, M. A.; Khandasammy, S. R.; Lednev, I. K. *Anal. Chem.* **2019**, *91* (1), 637−654.
(112) Yang, J.-H.; Choi, S.-J.; Yoh, J. J. *Spectrochim. Acta Part B At. Spectrosc.* **2017**, *134*, 25−32.
(113) Yang, J.-H.; Yoh, J. J. *Microchem. J.* **2018**, *139*, 386−393.
(114) Hilario, F. F.; Mello, M. L. de; Pereira-Filho, E. R. *Anal. Methods* **2021**, *13* (2), 232−241.
(115) Yin, P.; Yang, E.; Chen, Y.; Peng, Z.; Li, D.; Duan, Y.; Lin, Q. *Chem. Commun.* **2021**, *57* (59), 7312−7315.
(116) Moncayo, S.; Trichard, F.; Busser, B.; Sabatier-Vincent, M.; Pelascini, F.; Pinel, N.; Templier, I.; Charles, J.; Sancey, L.; Motto-Ros, V. *Spectrochim. Acta Part B At. Spectrosc.* **2017**, *133*, 40−44.
(117) Busser, B.; Moncayo, S.; Trichard, F.; Bonneterre, V.; Pinel, N.; Pelascini, F.; Dugourd, P.; Coll, J. L.; D'Incan, M.; Charles, J.; Motto-Ros, V.; Sancey, L. *Mod. Pathol* **2018**, *31* (3), 378−384.
(118) Modlitbová, P.; Pořízka, P.; Kaiser, J. *TrAC Trends Anal. Chem.* **2020**, *122*, 115729.
(119) Ilhardt, P. D.; Nuñez, J. R.; Denis, E. H.; Rosnow, J. J.; Krogstad, E. J.; Renslow, R. S.; Moran, J. J. *Soil Biol. Biochem.* **2019**, *131*, 119−132.
(120) de Oliveira, A. P.; de Oliveira Leme, F.; Nomura, C. S.; Naozuka, J. *Sci. Rep.* **2019**, *9* (1), 10827.
(121) Singh, V. K.; Tripathi, D. K.; Mao, X.; Russo, R. E.; Zorba, V. *Appl. Spectrosc.* **2019**, *73* (4), 387−394.
(122) Peng, J.; He, Y.; Zhao, Z.; Jiang, J.; Zhou, F.; Liu, F.; Shen, T. *Environ. Pollut.* **2019**, *252*, 1125−1132.
(123) Dell'Aglio, M.; Alrifai, R.; De Giacomo, A. *Spectrochim. Acta Part B At. Spectrosc.* **2018**, *148*, 105−112.
(124) Zhao, X.; Zhao, C.; Du, X.; Dong, D. *Sci. Rep.* **2019**, *9* (1), 906.
(125) Modlitbová, P.; Pořízka, P.; Střítežská, S.; Zezulka, Š.; Kummerová, M.; Novotný, K.; Kaiser, J. *Chemosphere* **2020**, *251*, 126174.
(126) Le Guevel, X.; Henry, M.; Motto-Ros, V.; Longo, E.; Montanez, M. I.; Pelascini, F.; de La Rochefoucauld, O.; Zeitoun, P.; Coll, J. L.; Josserand, V.; Sancey, L. *Nanoscale* **2018**, *10* (39), 18657−18664.
(127) Busser, B.; Bulin, A.-L.; Gardette, V.; Elleaume, H.; Pelascini, F.; Bouron, A.; Motto-Ros, V.; Sancey, L. *J. Neurosci. Methods* **2022**, *379*, 109676.
(128) Meng, Y.; Gao, C.; Lin, Z.; Hang, W.; Huang, B. *Nanoscale Adv.* **2020**, *2* (9), 3983−3990.
(129) Galbács, G.; Kéri, A.; Kohut, A.; Veres, M.; Geretovszky, Zs. *J. Anal. At. Spectrom.* **2021**, *36* (9), 1826−1872.
(130) Hartnell, D.; Andrews, W.; Smith, N.; Jiang, H.; McAllum, E.; Rajan, R.; Colbourne, F.; Fitzgerald, M.; Lam, V.; Takechi, R.; Pushie, M. J.; Kelly, M. E.; Hackett, M. J. *Front. Neurosci.* **2020**, *13*, 1415.
(131) Lin, Q.; Wang, S.; Duan, Y.; Tuchin, V. V. *J. Biophotonics* **2021**, *14* (5), No. e202000479.
(132) Bulin, A.-L.; Broekgaarden, M.; Chaput, F.; Baisamy, V.; Garrevoet, J.; Busser, B.; Brueckner, D.; Youssef, A.; Ravanat, J.-L.; Dujardin, C.; Motto-Ros, V.; Lerouge, F.; Bohic, S.; Sancey, L.; Elleaume, H. *Adv. Sci.* **2020**, *7* (20), 2001675.
(133) Kalot, G.; Godard, A.; Busser, B.; Pliquett, J.; Broekgaarden, M.; Motto-Ros, V.; Wegner, K. D.; Resch-Genger, U.; Köster, U.; Denat, F.; Coll, J.-L.; Bodio, E.; Goze, C.; Sancey, L. *Cells* **2020**, *9* (9), 1953.
(134) Manard, B. T.; Hintz, C. J.; Quarles, C. D.; Burns, W.; Zirakparvar, N. A.; Dunlap, D. R.; Beiswenger, T.; Cruz-Uribe, A. M.; Petrus, J. A.; Hexel, C. R. *Metallomics* **2022**, *14* (7), mfac050.
(135) Xu, F.; Ma, S.; Zhao, C.; Dong, D. *Front. Phys.* **2022**, *10*, 7.
(136) Choi, J.-H.; Shin, S.; Moon, Y.; Han, J.; Hwang, E.; Jeong, S. *Spectrochim. Acta Part B At. Spectrosc.* **2021**, *179*, 106090.
(137) Kiss, K.; Šindelářová, A.; Krbal, L.; Stejskal, V.; Mrázová, K.; Vrábel, J.; Kaška, M.; Modlitbová, P.; Pořízka, P.; Kaiser, J. *J. Anal. At. Spectrom.* **2021**, *36* (5), 909−916.
(138) WMA - The World Medical Association. *WMA Declaration of Helsinki - Ethical Principles for Medical Research Involving Human Subjects*. https://www.wma.net/policies-post/wma-declaration-of-helsinki-ethical-principles-for-medical-research-involving-human-subjects/ (accessed 2022-11-01).
(139) Khan, M. N.; Wang, Q.; Idrees, B. S.; Xiangli, W.; Teng, G.; Cui, X.; Zhao, Z.; Wei, K.; Abrar, M. *Front. Phys.* **2022**, *10*, 821057.
(140) Yin, P.; Hu, B.; Li, Q.; Duan, Y.; Lin, Q. *IEEE Trans. Instrum. Meas.* **2021**, *70*, 1−7.

(141) University Hospital, Grenoble. *Multi-Elemental Imaging of Lung Tissues With LIBS (Laser-Induced Breakdown Spectroscopy) : A Feasibility Study*; Clinical trial registration NCT03901196; clinicaltrials.gov, 2022. https://clinicaltrials.gov/ct2/show/NCT03901196 (accessed 2022-08-31).
(142) Martinez, M.; Baudelet, M. *Anal. Bioanal. Chem.* **2020**, *412* (1), 27−36.
(143) Legnaioli, S.; Campanella, B.; Pagnotta, S.; Poggialini, F.; Palleschi, V. Chapter 24 - Self-Calibrated Methods for LIBS Quantitative Analysis. In *Laser-Induced Breakdown Spectroscopy*, 2nd ed.; Singh, J. P., Thakur, S. N., Eds.; Elsevier: Amsterdam, 2020; pp 561−580. DOI: 10.1016/B978-0-12-818829-3.00024-1.
(144) Motto-Ros, V.; Moncayo, S.; Trichard, F.; Pelascini, F. *Spectrochim. Acta Part B At. Spectrosc.* **2019**, *155*, 127−133.
(145) Nardecchia, A.; Motto-Ros, V.; Duponchel, L. *Anal. Chim. Acta* **2021**, *1157*, 338389.
(146) Richiero, S.; Sandoval, C.; Oberlin, C.; Schmitt, A.; Lefevre, J.-C.; Bensalah-Ledoux, A.; Prigent, D.; Coquidé, C.; Valois, A.; Giletti, F.; Pelascini, F.; Duponchel, L.; Dugourd, P.; Comby-Zerbino, C.; Motto-Ros, V. *Appl. Spectrosc.* **2022**, *76* (8), 978−987.
(147) Moncayo, S.; Duponchel, L.; Mousavipak, N.; Panczer, G.; Trichard, F.; Bousquet, B.; Pelascini, F.; Motto-Ros, V. *J. Anal. At. Spectrom.* **2018**, *33* (2), 210−220.
(148) Finotello, R.; Tamaazousti, M.; Sirven, J.-B. *Spectrochim. Acta Part B At. Spectrosc.* **2022**, *192*, 106418.
(149) Nardecchia, A.; Fabre, C.; Cauzid, J.; Pelascini, F.; Motto-Ros, V.; Duponchel, L. *Anal. Chim. Acta* **2020**, *1114*, 66−73.
(150) Wu, Q.; Marina-Montes, C.; Cáceres, J. O.; Anzano, J.; Motto-Ros, V.; Duponchel, L. *Spectrochim. Acta Part B At. Spectrosc.* **2022**, *195*, 106508.
(151) Meima, J. A.; Rammlmair, D. *Chem. Geol.* **2020**, *532*, 119376.
(152) Müller, S.; Meima, J. A. *Spectrochim. Acta Part B At. Spectrosc.* **2022**, *189*, 106370.
(153) Choi, J.-H.; Shin, S.; Moon, Y.; Han, J. H.; Hwang, E.; Jeong, S. *Spectrochim. Acta Part B At. Spectrosc.* **2021**, *179*, 106090.
(154) Casado-Gavalda, M. P.; Dixit, Y.; Geulen, D.; Cama-Moncunill, R.; Cama-Moncunill, X.; Markiewicz-Keszycka, M.; Cullen, P. J.; Sullivan, C. *Talanta* **2017**, *169*, 123−129.
(155) Dixit, Y.; Casado-Gavalda, M. P.; Cama-Moncunill, R.; Cama-Moncunill, X.; Markiewicz-Keszycka, M.; Cullen, P. J.; Sullivan, C. *Anal. Methods* **2017**, *9* (22), 3314−3322.
(156) Cama-Moncunill, X.; Markiewicz-Keszycka, M.; Dixit, Y.; Cama-Moncunill, R.; Casado-Gavalda, M. P.; Cullen, P. J.; Sullivan, C. *Food Control* **2017**, *78*, 304−310.
(157) Sandoval-Muñoz, C.; Velásquez, G.; Álvarez, J.; Pérez, F.; Velásquez, M.; Torres, S.; Sbarbaro-Hofer, D.; Motto-Ros, V.; Yáñez, J. *J. Anal. At. Spectrom.* **2022**, *37* (10), 1981−1993.
(158) El Haddad, J.; de Lima Filho, E. S.; Vanier, F.; Harhira, A.; Padioleau, C.; Sabsabi, M.; Wilkie, G.; Blouin, A. *Miner. Eng.* **2019**, *134*, 281−290.
(159) Nardecchia, A.; de Juan, A.; Motto-Ros, V.; Gaft, M.; Duponchel, L. *Anal. Chim. Acta* **2022**, *1192*, 339368.
(160) Pagnotta, S.; Lezzerini, M.; Ripoll-Seguer, L.; Hidalgo, M.; Grifoni, E.; Legnaioli, S.; Lorenzetti, G.; Poggialini, F.; Palleschi, V. *Appl. Spectrosc.* **2017**, *71* (4), 721−727.
(161) Pagnotta, S.; Lezzerini, M.; Campanella, B.; Gallello, G.; Grifoni, E.; Legnaioli, S.; Lorenzetti, G.; Poggialini, F.; Raneri, S.; Safi, A.; Palleschi, V. *Spectrochim. Acta Part B At. Spectrosc.* **2018**, *146*, 9−15.
(162) Chen, T.; Sun, L.; Yu, H.; Wang, W.; Qi, L.; Zhang, P.; Zeng, P. *Appl. Geochem.* **2022**, *136*, 105135.
(163) Gaft, M.; Nagli, L.; Raichlin, Y.; Pelascini, F.; Panzer, G.; Ros, V. M. *Spectrochim. Acta Part B At. Spectrosc.* **2019**, *157*, 47−52.
(164) Gaft, M.; Nagli, L.; Gornushkin, I.; Raichlin, Y. *Spectrochim. Acta Part B At. Spectrosc.* **2020**, *173*, 105989.
(165) Clavé, E.; Gaft, M.; Motto-Ros, V.; Fabre, C.; Forni, O.; Beyssac, O.; Maurice, S.; Wiens, R. C.; Bousquet, B. *Spectrochim. Acta Part B At. Spectrosc.* **2021**, *177*, 106111.

https://doi.org/10.1021/acs.analchem.2c04910
Anal. Chem. 2023, 95, 49−69